Journal of Intelligent Material Systems and Structures

http://jim.sagepub.com

Electrical-resistance-based Sensing of Impact Damage in Carbon Fiber Reinforced Cement-based Materials

David G. Meehan, Shoukai Wang and D.D.L. Chung

Journal of Intelligent Material Systems and Structures 2010; 21; 83 originally published online Nov 23, 2009;
DOI: 10.1177/1045389X09354786

The online version of this article can be found at:
http://jim.sagepub.com/cgi/content/abstract/21/1/83

Published by:
SAGE
http://www.sagepublications.com

Electrical-resistance-based Sensing of Impact Damage in Carbon Fiber Reinforced Cement-based Materials

DAVID G. MEEHAN, SHOUKAI WANG AND D. D. L. CHUNG*

Composite Materials Research Laboratory, University at Buffalo
State University of New York, Buffalo, NY 14260-4400, USA

ABSTRACT: Damage monitoring of the civil infrastructure is critically needed. This article provides the first report of impact damage self-sensing in cement-based materials. Cement mortar reinforced with short (5–7 mm) carbon fiber and in bulk or coating (5–10 mm thick) form is effective for sensing its own impact damage through DC/AC electrical resistance measurement, provided that the region of resistance measurement contains the point of impact. The mortar resistivity needs to be 10^4–10^5 Ω cm, as provided by pitch-based fiber (15 μm diameter, unsized) at 0.5% or 1.0% by mass of cement, or type A PAN-based fiber (7 μm diameter, desized) at 0.5%. Due to the low mortar resistivity of 10^3 Ω cm, pitch-based fiber at 1.5% and type B PAN-based fiber (7 μm diameter, unsized) at 0.5% are less effective. Without fiber, there is no sensing ability. The surface resistance of the surface receiving the impact is an effective indicator of the damage, even for minor damage without cracking, inflicted by impact at 880 J. The oblique or longitudinal volume resistance is much less effective. The surface resistance increases abruptly upon impact, but it decreases abruptly upon impact after 5–40 impacts (number decreasing with increasing impact energy) have been inflicted.

Key Word: cement, concrete, carbon fiber, sensing, damage, impact, electrical resistance, electrical resistivity.

INTRODUCTION

DUE to the aging of the civil infrastructure, monitoring of damage in concrete structures is of national importance. Self-sensing refers to the ability of a structural material to sense its own structural attributes, such as damage and strain (Chung, 2003, 2004). This is in contrast to the use of embedded or attached sensors, which are more costly and less durable than the structural material. Furthermore, the use of an embedded sensor can lead to mechanical property loss.

The self-sensing of strain, damage and temperature has been reported in cement-based materials containing short carbon fibers (Chen and Chung, 1993a,b, 1996; Fu and Chung, 1995, 1996, 1997; Bontea et al., 2000; Chung, 2002a,b, 2003; Wen and Chung, 2000, 2001a,b, 2003, 2005, 2006a, 2007a,b; Yao et al., 2003; Reza et al., 2003). The fibers are typically used at a volume fraction below the percolation threshold. (The percolation threshold is the volume fraction above which the fibers touch one another to form a continuous electrical conduction path.) The fibers are not the sensor. Rather, they are an admixture that renders self-sensing ability to the cement-based material. In addition, the fibers enhance the flexural strength, flexural toughness, tensile strength, and tensile ductility, in addition to reducing the drying shrinkage (Chung, 2002b).

The self-sensing of strain and damage has been shown in carbon fiber cement-based materials under tension, compression, and flexure (Wen and Chung, 2000, 2001a, 2006a,b,c,d). The loading schemes include static loading up to failure as well as repeated loading at various stress amplitudes. The self-sensing ability relates to the change in the electrical resistivity upon strain or damage. Reversible strain (i.e., strain in the elastic regime) results in a reversible change in the resistivity. The volume resistivity increases in both the longitudinal and transverse directions upon uniaxial tension; it decreases in both the longitudinal and transverse directions upon uniaxial compression. Under flexure, the oblique resistance (volume resistance in a direction between the longitudinal and through-thickness directions) increases, while the surface resistance on the compression side decreases and the surface resistance on the tension side increases. Under all these forms of loading, damage causes an irreversible increase of the resistance. Under flexure, the surface resistance on the tension side is particularly sensitive to damage.

*Author to whom correspondence should be addressed.
E-mail: ddlchung@buffalo.edu
Figures 10, 17, 22, 23 and 25 appear in color online: http://jim.sagepub.com

1045-389X/10/01 0083–23 $10.00/0 DOI: 10.1177/1045389X09354786

In spite of the prior work mentioned above, no work has been reported on the self-sensing of impact damage in cement-based materials. This article provides the first report of this subject. On the other hand, the self-sensing of impact damage has been shown in continuous carbon fiber epoxy-matrix composites, using electrical resistance measurement (Wang and Chung, 2005; Wang et al., 2005a,b,c, 2006a,b,c,d; Wang and Chung, 2006). Continuous carbon fiber epoxy-matrix composites differ greatly from cement-based materials in their low electrical resistivity in the fiber direction of the composite, and in their electrical and mechanical anisotropy. Due to the discontinuity of the carbon fiber in a cement-based material, the electrical resistivity is high and the material is essentially isotropic. The high resistivity makes resistance-based damage sensing more challenging, but the isotropy makes it simpler. Impact is a widely encountered form of loading. For example, impact is encountered when a car hits a structure on a road, when an airplane hits an airport runway, when cargo is dropped on a yard, when an ocean wave hits a pier, when an earthquake or an explosion occurs, etc.

Damage distribution can be in the form of a region that is damaged and surrounded by a region that is not damaged at all. It can also be in the form of a region of severe damage, surrounded by a region of less damage, such that the severity of the damage in the surrounding region decreases with increasing distance from the region of severe damage. The former scenario applies to localized damage, as in impact damage. The latter scenario applies to delocalized damage, as in flexural damage, in which the flexural stress distribution gives rise to a damage distribution that is spread out.

The sensing of localized damage can be achieved by measuring the resistance of the damaged region. It cannot be achieved by measuring the resistance outside the damaged region, since the region outside the damaged region is not damaged. In contrast, the sensing of delocalized damage can be achieved by measuring the resistance in the region of severe damage or the surrounding region of less damage.

This work is directed to developing the technology that allows cement-based materials to sense their own impact damage. Specific aims include: (i) assessing the ability of carbon fiber cement mortar in bulk and coating forms, to sense its own localized damage that is due to impact; (ii) studying the effects of damage degree and damage history on the sensing ability; (iii) investigating the effects of the size and location of the sensed region on the effectiveness of impact damage sensing; (iv) developing the electrical resistance measurement method (surface resistance vs. volume resistance; AC vs. DC; four-probe vs. two-probe methods) for sensing the impact damage; (v) providing a comparative evaluation of different types and proportions of carbon fiber for the sensing; (vi) understanding the sensing ability in terms of the electrical resistivity change of the damaged region; and (vii) correlation of the resistance change and the flexural strength loss due to the damage. Electrical measurement schemes evaluated pertain to those corresponding to the measurement of the longitudinal volume resistance (i.e., volume resistance in a direction along the length of the specimen, perpendicular to the direction of impact), the oblique volume resistance, and the surface resistance of the surface under impact.

EXPERIMENTAL METHODS

Materials

Three types of carbon fiber are evaluated, as described in Table 1. The pitch-based fibers (Ashland Petroleum Co., Ashland, KY, production discontinued) are used, unless otherwise noted. The type A polyacrylonitrile (PAN)-based fiber (carbon content 95%, Grade PANEX35CF0333-48, Zoltek Inc., Bridgeton, MO) is sized, thus requiring desizing. The type B PAN-based fiber (Grade PANEX33CF0250-01, production discontinued) is unsized, so desizing is not performed. (The application of the desizing treatment to type B is found to be detrimental to the sensing performance.) Prior to using the fibers in cement, they are prepared, as described in Table 2, for the purpose of desizing and/or ozone surface treatment. The ozone treatment involves exposure to ozone gas (0.6 vol.%, in oxygen) is for improving the wettability of fibers by water (Wen and Chung, 2005).

Fibers in amounts of 0, 0.50, 1.00, and 1.50% by mass of cement (corresponding to 0, 0.24, 0.48, and 0. vol.% of mortar) were used. Unless noted otherwise, the fiber content is 0.50% by mass of cement. In case of the pitch-based fibers (15 μm diameter, Table 1) in cement paste, the percolation threshold is between 0.5 and 1.0 vol.% (Chen and Chung, 1995). In case of pitch-based fibers (7 μm diameter) of prior work, the percolation threshold is between 0.4 and 0.8 vol.%, both in cement paste and in mortar with sand/cement ratio 1.0 (Chen et al., 2004).

The cement used is Portland cement (Type I) from Lafarge Corp. (Southfield, MI). The sand used is natural sand (100% passing 2.36 mm sieve, 99.9% SiO_2). The sand/cement ratio is 1.0. The water/cement ratio is 0.35. A water reducing agent (WR) is used in the amount of 3% by weight of cement. The WR is TAMOL SN (Rohm and Haas, Philadelphia, PA), which contains 93–96% sodium salt of a condensed naphthalene sulfonic acid. No coarse aggregate is used. These ingredients and their proportions are the same for the plain mortar as well as the carbon fiber reinforced mortar.

The following ingredients are used in the carbon fiber mortar mix. Silica fume (Elkem Materials Inc., Pittsburgh, PA, microsilica, EMS 965) is used in the amount of 15% by mass of cement. The methylcellulose,

Table 1. Three types of carbon fibers used in this work.

Fiber type	Source	Sizing	Diameter (μm)	Length (mm)	Resistivity ($10^{-3}\,\Omega\,cm$)	Tensile strength (MPa)	Tensile modulus (GPa)	Elongation (%)	Density (g/cm^3)
Pitch-based	Ashland*	Unsized	15	5	3.0	690	48	1.4	1.6
Type A PAN-based	Zoltek	Urethane-based	7.2	8	1.55	3,800	242	1.5	1.81
Type B PAN-based	Zoltek	Unsized	7.2	8	1.55	3,800	228	1.5	1.81

*Discontinued.

Table 2. Methods of preparing carbon fiber prior to incorporation in the cement mix.

Fiber type	Step 1	Step 2
Pitch-based	Dry for 1 h at 110°C	Ozone treat for 10 min at 160°C
Type A PAN-based	Desize for 4 h at 500°C	Ozone treat for 10 min at 160°C*
Type B PAN-based	Dry for 1 h at 110°C	Ozone treat for 10 min at 160°C

*Immediately after Step 1, the fiber is cooled to 160°C for ozone treatment.

used in the amount of 0.4% by mass of cement, is Dow Chemical Corp., Midland, MI, Methocel A15-LV. The defoamer (Colloids Inc., Marietta, GA, 1010) is in the amount of 0.13 vol.% (% of specimen volume).

A rotary mixer with a flat beater is used for mixing. Methylcellulose is dissolved in water and then the defoamer and fibers are added, and stirred by hand for about 2 min. Then, the methylcellulose mixture, cement, water, and silica fume are mixed for 5 min. After pouring the mix into oiled molds, an external electric vibrator is used to facilitate compaction and decrease the amount of air bubbles. The specimens are demolded after 1 day and then allowed to cure at room temperature in air (relative humidity = 100%) for 28 days. Three specimens are tested to confirm the reproducibility of each type of testing result.

Unless noted otherwise, all specimens are in the form of a rectangular monolith of size $160 \times 40 \times 40\,mm^3$, which is the size of the mold cavity. However, for the purpose of studying carbon fiber mortar in the form of a coating, some specimens are in the form of a layer of carbon fiber reinforced mortar on top of a rectangular monolith of plain mortar (without fiber, silica fume or methylcellulose). The plain mortar is mixed and then poured into the oiled mold ($160 \times 40 \times 40\,mm^3$) to the appropriate height for testing. This height is obtained by subtracting the desired conductive layer thickness (0.25, 1.0, 1.5, 2.0, 2.5, or 5.0 mm) from the mold height (40 mm). Then the mixing equipment is cleaned and the carbon fiber reinforced mortar is mixed and poured into the mold. An average of 20 min elapses between the time the plain mortar layer is smoothed and the carbon fiber mortar layer is poured. The finished size of a specimen with the overlayer is identical to the size of the homogeneous specimen.

The base of the impact testing apparatus is a solid cube of steel, with each side of the cube measuring approximately 15 cm. Fastened to the base and positioned at two diagonally opposite corners of the top surface of the cube are two cylindrical rods that are used to guide the vertical motion of the indenter. Friction between the indenter assembly and guides is reduced by the application of lubricating oil. The specimen sits flat on the base, centered between the guide rods, with the length of the specimen being perpendicular to the diagonal mentioned above, such that the indenter is above the center of the top surface of the specimen.

Testing Methods

DC electrical resistance is measured using a Keithley Model 2001 multimeter. The current is 89 μA when the resistance is 2–20 kΩ and is 0.98 mA when the resistance is 0.2–2.0 kΩ. The resistance encountered in this work is mostly in the former range.

In order to investigate the effect of electrical contact configuration on the sensing effectiveness, electrical contacts with different configurations (Figures 1–4) are applied to different specimens after the specimens have been cured for 28 days.

Unless noted otherwise, the four-probe method is used for DC resistance measurement. In this method, there are four electrical contacts, with outer two probes (A and D in Figures 1, 2, and 4) for passing current and inner two probes (B and C in Figures 1, 2, and 4) for voltage measurement. For the sake of comparison, the two-probe method is also evaluated. In the two-probe method (Figure 3), there are two electrical contacts, with each of them used for both passing current and measuring the voltage.

In the four-probe method, by having separate contacts for the current and the voltage, there is essentially no potential drop at each voltage contact, thereby allowing the measured voltage between the voltage contacts to

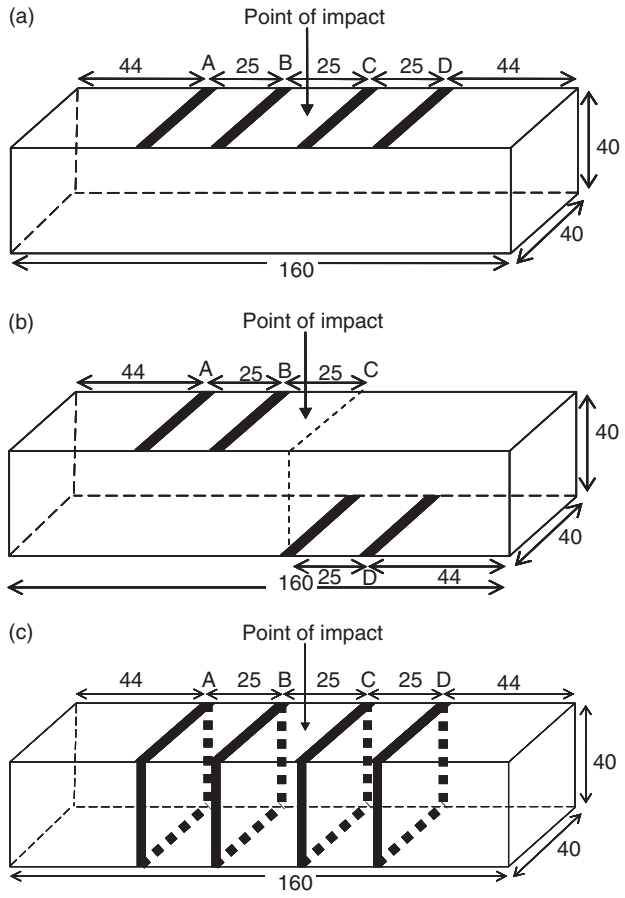

Figure 1. *Electrical contact configurations for measurement of the electrical resistance of the segment that contains the point of impact: (a) surface resistance measurement, (b) oblique volume resistance measurement, (c) longitudinal volume resistance measurement. In all cases, A and D are electrical contacts for passing current, while B and C are electrical contacts for voltage measurement. All dimensions are in mm.*

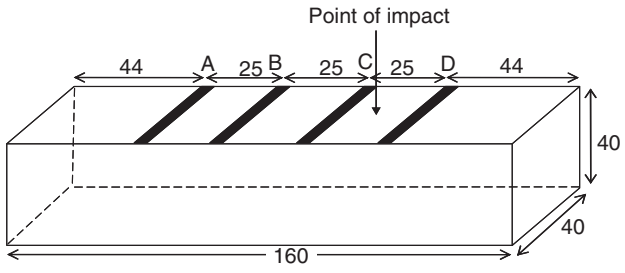

Figure 2. *Electrical contact configuration for measurement of the surface resistance of the segment that does not contain the point of impact. All dimensions are in mm.*

be the voltage drop within the specimen, without including the voltage drop at each voltage contact. The quality of electrical contacts varies, depending on the microstructure of the interface between the contact material and the specimen surface. As a consequence, the resistance associated with an electrical contact varies among different contacts – even different contacts on the same specimen. Due to this variability, it is important to

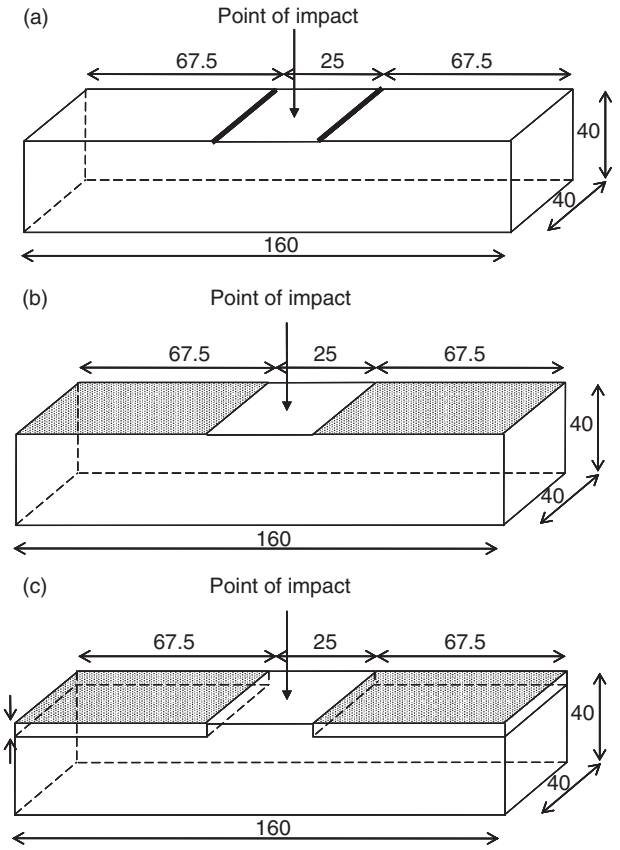

Figure 3. *Two-probe electrical contact configuration used to investigate different probe surface areas. (a) is the standard two-probe configuration. (b) is a sample contact configuration consisting of silver paint across the top surface of the sample. (c) is a contact configuration involving steel wool embedded into the top 7.5 mm part of the specimen. All dimensions are in mm.*

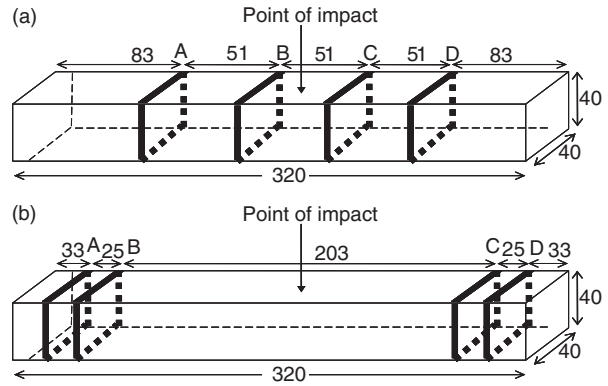

Figure 4. *Electrical contact configuration for measurement of the longitudinal volume resistivity for the larger specimen size: (a) distance of 51 mm between the voltage contacts, (b) distance of 203 mm between the voltage contacts. All dimensions are in mm.*

decouple the contact resistance from the specimen resistance through the use of the four-probe method. The four-probe method is advantageous compared to the two-probe method in that it does not include the resistance of the electrical contacts in the measured resistance, whereas the two-probe method gives a resistance, which includes the contact resistance.

Three four-probe electrical contact configurations are used, as illustrated in Figure 1, for measuring the surface resistance (Figure 1(a)); the oblique volume resistance (Figure 1(b)); and the longitudinal volume resistance (Figure 1(c)). In each of the configurations in Figure 1, the outer two contacts, labeled A and D, are for passing current, while the inner two contacts, labeled B and C, are for voltage measurement.

The longitudinal volume resistance is the resistance along the length of the specimen, as obtained by using electrical contacts that are perimetric around the entire specimen at different planes that are perpendicular to the longitudinal direction (Figure 1(c)). The perimetric current contacts allow the current to penetrate the entire cross-section of the specimen in the region between the voltage contacts, which is the region of resistance measurement.

The surface resistance is the resistance of the top surface region in the longitudinal direction, as obtained by using electrical contacts that are on the top surface only (Figure 1(a)). The current contacts located on the top surface allow the current to penetrate for a limited depth into the specimen. In general, the depth of current penetration increases with decreasing resistivity of the specimen. In this work, the top surface is the side receiving the impact.

The oblique direction is a direction that is between the longitudinal and through-thickness directions. The resistance in the oblique direction is obtained by using two electrical contacts on each of the two opposite surfaces of the specimen, such that the contacts on the two surfaces are not directly opposite. The four electrical contacts used in measuring the oblique resistance are not collinear, so that the current direction (AD) and voltage direction (BC) do not exactly overlap. Thus, this is not the ideal four-probe method. Furthermore, the cross-sectional area of the oblique current path is not well defined and, as a result, the resistivity cannot be determined. Nevertheless, the configuration is effective for providing a resistance value that is meaningful on a relative scale, so that the method is effective for sensing damage, as shown in prior work on the sensing of impact damage on continuous carbon fiber epoxy-matrix composites (Wang et al., 2005b).

The oblique resistance is attractive for detecting interior damage, whereas the surface resistance is sensitive to surface damage. The longitudinal volume resistance is also sensitive to the interior damage, but the implementation of the perimetric contacts is inconvenient for a large concrete structure. In this work, comparison is made among these three methods of resistance measurement in relation to the effectiveness for sensing impact damage in cement-based materials.

Silver paint is a suspension of silver particles in a volatile solvent (Leong and Chung, 2006; Wang et al., 2007). Upon evaporation of the solvent, the silver particles touch one another, thereby providing high electrical conductivity. Silver paint is the electrical contact material used, unless noted otherwise. It is applied manually on the surface of the specimen and then allowed to dry in air at room temperature. Although silver paint is used in conjunction with copper wire, it is the silver paint that is in direct contact with the cement-based material. Due to the limited conformability of the copper wire to the surface topography of the cement-based material, a conductive paste such as silver paint is necessary.

An electrical contact may be in the form of a line, which is on the specimen surface and is oriented in a direction perpendicular to the longitudinal direction (which is the direction of resistance measurement), and extends for the entire width of the specimen, as illustrated in Figures 1, 2, 3(a), and 4. The contact may alternatively be in the form of an area, such as the rectangular area that extends for the entire width of the specimen, as illustrated in Figure 3(b). The area contact of Figure 3(b) is advantageous over the line contact of Figure 3(a), because the former has a larger area and hence a lower contact resistance. The area is 220 mm^2 for the line contact in Figure 3(a), but is 2720 mm^2 for the area contact in Figure 3(b). A small value of the contact resistance is more important in the two-probe method than the four-probe method. Therefore, in this work, the area contacts are used only for the two-probe method (Figure 3(b)).

In order to further increase the area of the interface between the electrical contact material and the cement-based material, so as to further decrease the contact resistance in the two-probe method, stainless steel wool (as used in the kitchen, with a wire diameter of 0.02 mm) embedded in the surface region of a cement-based specimen is alternatively used (in place of silver paint) as the electrical contact material. An end of the wool is allowed to protrude from the surface of the specimen in order to facilitate electrical connection. The embedded area is rectangular, as illustrated in Figure 3(c). Mixing and pouring of the cement mix are conducted as described above. After pouring in a mold, the steel wool is embedded into the top surface, and the top surface is then smoothed manually. The embedment depth is about 7.5 mm.

The region of resistance measurement is the region bound by the two voltage contacts. The distance between the voltage contacts may affect the sensitivity of detecting damage that is localized at and around the point of impact, which is in the region bound by the voltage contacts. For the purpose of studying the effect of the distance of the voltage contacts from the point of impact on the effectiveness of impact damage sensing, a large specimen size of $320 \times 40 \times 40\,mm^3$ is used (Figure 4). The large size has twice the length of the specimens in Figures 1–3. The long length of the

specimen in Figure 4 allows the voltage contact separation to vary greatly, namely from 51 mm in Figure 4(a) to 203 mm in Figure 4(b). For the larger specimen size, only the longitudinal volume resistance was measured, using perimetric contacts.

Before, during, and after impact using a steel hemisphere (19 mm or 0.75 in. diameter), which is dropped from a controlled height, resistance measurement is made. Unless noted otherwise, the point of impact is centered between the voltage contacts. The impact energy is calculated from the mass of the hemisphere assembly (0.740 kg) and the initial height of the hemisphere (up to 850 mm). The impact is directed at the same point of the specimen (as indicated in Figures 1–4) at various energies. Unless noted otherwise, the impact energy is progressively increased in steps. The impact area of the specimen is electrically insulated from the steel hemisphere by using plastic adhesive tape. The highest impact energy used is 3990 J, which is below the energy of 4650 J needed to fracture the specimen. The extent of bouncing back of the hemisphere after impact is so small that essentially all of the initial potential energy of the hemisphere is transferred to the specimen.

Electrical resistance data is acquired at a rate such that 0.1 s elapses between successive data points. The time of data collection is about 6 s for each impact. About half of the time period is before the impact and the remaining time is after the impact. The resistance measurement is stopped for about 1 min between successive impacts. Unless noted otherwise, the resistance measured is the surface resistance, as obtained by using the four-probe method, Figure 1(a).

Unless noted otherwise, electrical resistance measurement is conducted under DC condition, using a Keithley Model 2001 multimeter. For the sake of comparison, AC impedance measurement is conducted using a precision LCR meter (Quadtech Model 7600) at 1 kHz. In AC testing, the quantity measured is R_s, which is the resistance based on an equivalent circuit consisting of a resistor and a capacitor in series.

In order to assess the damage using a method that is independent of the electrical resistance method, the flexural strength is measured before and after impact. This is conducted under three-point bending (span = 140 mm) up to failure. The testing is conducted before any impact and after impact at various chosen energies. A hydraulic mechanical testing system (MTS Systems Corp., Marblehead, MA) is used at a crosshead displacement speed of 0.5 mm/min. Three specimens are tested for each impact energy. The flexural roughness is taken as the area under the curve of flexural stress versus midspan deflection up to a flexural stress of 0.15 MPa (10 lb load).

The impacted region is examined by scanning electron microscopy and optical microscopy in order to characterize the dimensions and morphology of any indent or crack that may be present. The depth of the indent, as calculated from the measured radius of the indent and the geometry of the indenter, is shown in Table 3 for progressively increasing impact energy in the case of the pitch-based carbon fiber.

Table 4 shows that the resistance/resistivity before any impact decreases with increasing carbon fiber content. At the same fiber content, the oblique resistance is higher than the surface resistance.

RESULTS AND DISCUSSION

Sensing Impact at Progressing Increasing Energy, based on the Top Surface Resistance

Figure 5(a) shows the top surface resistance of each of two specimens containing the pitch-based carbon fiber upon impact at progressively increasing impact energy (shown in Table 3), as measured using the electrical contact configuration shown in Figure 1(a). The resistance increases abruptly and irreversibly upon impact at low energies (up to 2660 J), and decreases upon impact at high energies (3100 J and above). Figure 5(b) shows a magnified view of the 2660 J impact from Figure 5(a) and illustrates the abrupt and irreversible nature of the resistance increase. The fractional change in resistance is

Table 3. Impact energy and corresponding drop height of indenter and indent depth. The fiber is pitch-based.

Impact height (in)	Impact energy (J)	Indent depth (μm)
4	880	0
6	1330	1
8	1770	8
10	2200	21
12	2660	64
14	3100	82
16	3550	130
18	3990	171

Table 4. Resistance/resistivity before any impact for combinations of three resistance types and four carbon fiber contents. The fiber is pitch-based. The four-probe method is used.

	Resistance ($10^3\,\Omega$)		Resistivity (Ω cm)
Carbon fiber (% by mass of cement)	Top surface (Figure 1(a))	Oblique (Figure 1(b))	Perimetric (Figure 1(c))
0.0	11.92 ± 0.24	19.50 ± 0.02	$(5.98 \pm 0.31) \times 10^5$
0.5	2.97 ± 0.13	4.85 ± 0.01	$(1.61 \pm 0.24) \times 10^5$
1.0	0.16 ± 0.11	0.30 ± 0.01	$(1.77 \pm 0.22) \times 10^4$
1.5	0.03 ± 0.98	0.04 ± 0.01	$(2.28 \pm 0.22) \times 10^3$

33% for the end point of the sequence relative to the virgin state and is 200% for the highest resistance state in the sequence relative to the virgin state.

Figure 6(a) shows corresponding results for the top surface resistance of each of two specimens containing the type A PAN-based fiber. The resistance increases upon impact at low energies and decreases upon impact at high energies, as in Figure 5(a). The fractional change in resistance is 200% for the highest resistance point in the sequence relative to the virgin state.

Figure 7(a) shows corresponding results for top surface resistance of each of specimens containing the type B PAN-based fiber. The resistance is much lower than that for the type A PAN-based fiber, Figure 6(a), or the pitch-based fiber, Figure 5(a). The resistance increases abruptly upon impact at low impact energies (up to 2200 J), and remains essentially unaffected by subsequent impact at higher impact energies (3100 J and above). Figure 7(b) shows a magnified view of the 2660 J impact from Figure 7(a). The fractional change in resistance is 54% for the highest resistance point relative to the virgin state.

The fractional change in resistance is lower for the type B PAN-based fiber specimens than the type A PAN-based fiber specimens or the pitch-based fiber specimens. In addition, the decrease of the resistance before and after the abrupt rise in resistance that occurs upon impact is much more significant for the type B PAN-based fiber specimens than for the type A PAN-based fiber specimens and the pitch-based fiber specimens, as shown by the fact that the decreasing trend before and after each impact is much less in Figures 5 and 6, than in Figure 7. The resistance decreases before and after each impact is probably due to the resistance heating and the decrease of resistivity with increasing temperature (Wen and Chung, 1999). Resistance heating (Wang et al., 2004) is more significant for the type B PAN-based fiber specimens than the other two types of specimens, due to the lower resistivity of type B specimens (Figure 7). These differences, which mean that the type B PAN-based fiber is less suitable than the type A PAN-based fiber or the pitch-based fiber for resistance-based impact sensing, stem from the low resistivity of the specimens containing type B PAN-based fiber. The origin of the low resistivity of type B specimens is probably associated with a relatively high degree of fiber dispersion. The fiber dispersion is affected by the surface condition of the fiber. Type A is desized, whereas type B is unsized.

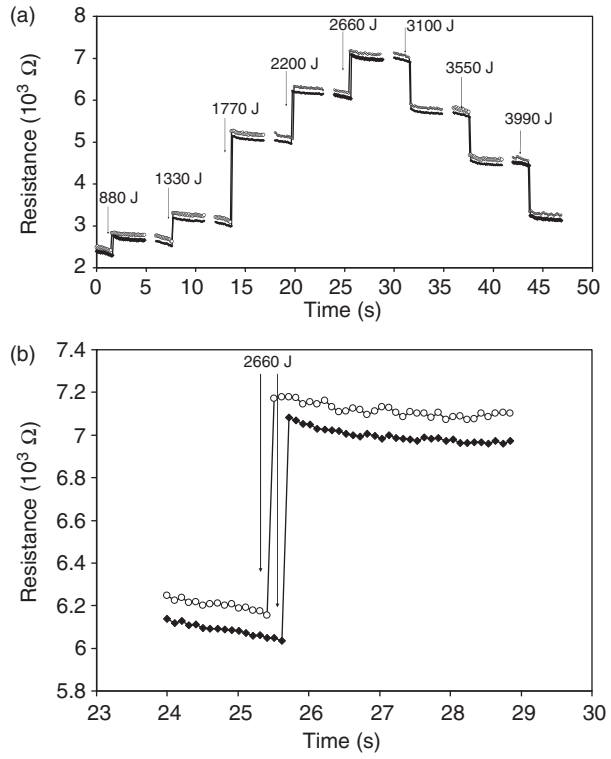

Figure 5. *Surface resistance (Figure 1(a)) upon progressively increasing impact energy. The impact energy is successively 880, 1330, 1770, 2200, 2660, 3100, 3550, and 3990 J. The two curves are for two specimens, each containing the pitch-based fiber at 0.50% by mass of cement. (b) is a magnified part of (a), showing the effect of impact at 2660 J.*

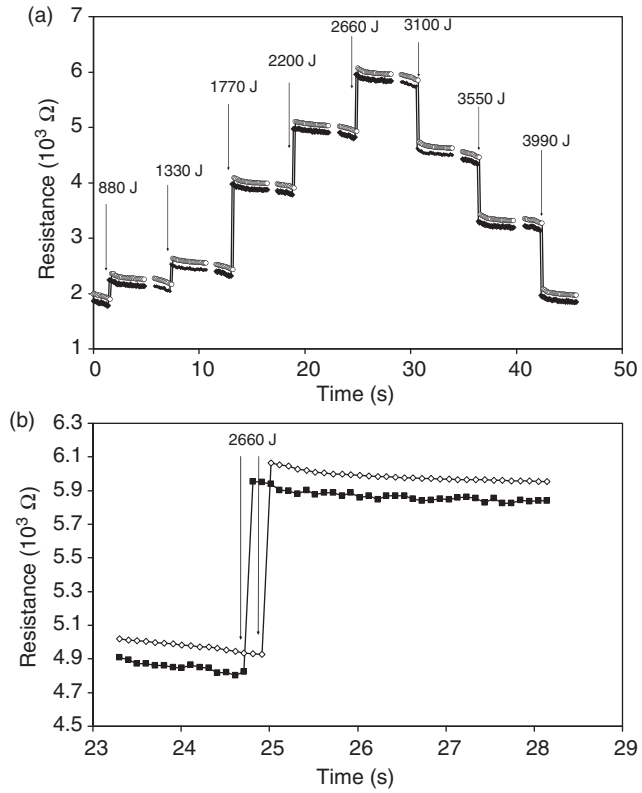

Figure 6. *Surface resistance (Figure 1(a)) upon progressively increasing impact energy. The impact energy is successively 880, 1330, 1770, 2200, 2660, 3100, 3550, and 3990 J. The two curves are for two specimens, each containing the type A PAN-based fiber at 0.50% by mass of cement. (b) is a magnified part of (a), showing the effect of impact at 2660 J.*

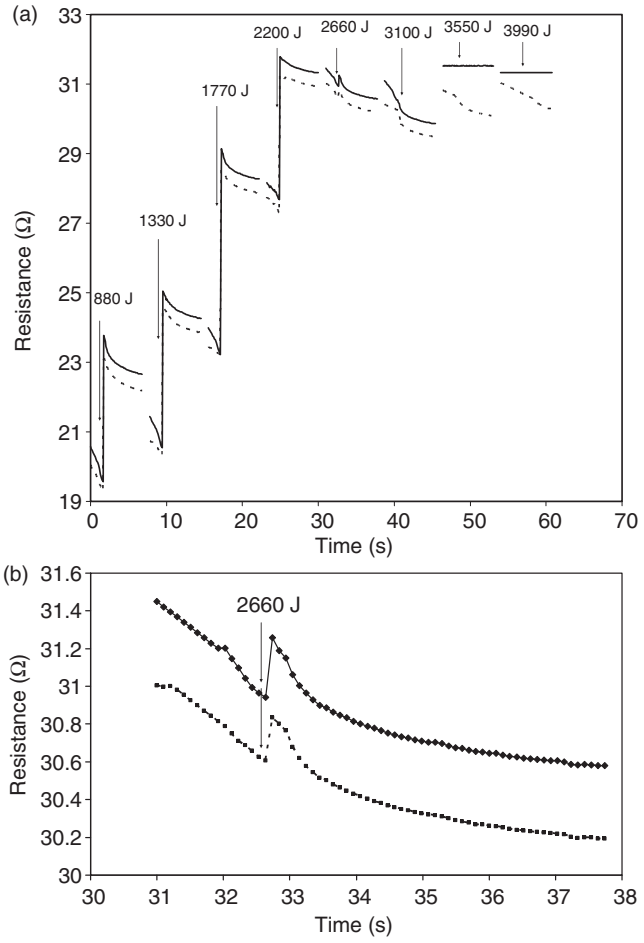

Figure 7. *Surface resistance (Figure 1(a)) upon progressively increasing impact energy. The impact energy is successively 880, 1330, 1770, 2200, 2660, 3100, 3550, and 3990 J. The two curves are for two specimens, each containing the type B PAN-based fiber at 0.50% by mass of cement. (b) is a magnified part of (a), showing the effect of impact at 2660 J.*

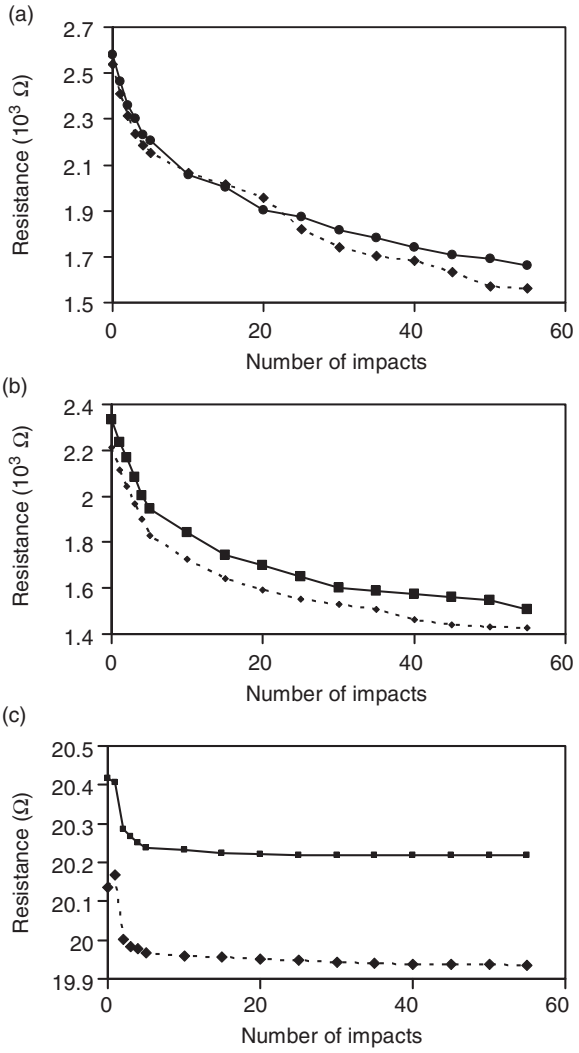

Figure 8. *Surface resistance (Figure 1(a)) upon repeated impact at a fixed energy of 3990 J. The two curves in each graph are for two specimens: (a) pitch-based fiber; (b) type A-PAN-based fibers; (c) type B PAN-based fiber.*

Sensing Repeated Impacts at a Fixed Energy, based on the Top Surface Resistance

Figure 8(a) shows the surface resistance of each of two pitch-based fiber specimens upon increasing numbers of impacts at the fixed energy of 3990 J, which is in the energy regime where the resistance decreases (rather than increasing) upon impact (Figure 5(a)). The resistance is measured by using the contact configuration of Figure 1(a). The resistance decreases monotonically with increasing number of impacts. The fractional decrease in resistance is about 37% relative to the virgin state for the largest number of impacts.

Figure 8(b) shows corresponding results for the type A PAN-based fiber specimens. The impact energy of 3990 J is in the energy regime where the resistance decreases (rather than increasing) upon impact (Figure 6(a)). The fractional decrease in resistance is 35% relative to the virgin state for the largest number of impacts.

Figure 8(c) shows corresponding results for the type B PAN-based fiber specimens. The impact energy of 3990 J is in the energy regime where the resistance essentially does not change upon impact (Figure 7(a)). The fractional decrease in resistance is 1% relative to the virgin state for the largest number of impacts. Thus, the type B PAN-based fiber is less effective than the type A PAN-based fiber or the pitch-based fiber for sensing repeated impacts at the same energy.

Figure 9 shows the effect of repeated impacts at a fixed energy for each of three energies (1330, 1770, and 2220 J). The pitch-based fiber is used. The resistance increases and then decreases with increasing number of impacts, such that the resistance attains a maximum at a larger number of impacts as the impact energy decreases. This trend is consistent with that for impacts at progressively increasing energy (Figure 5(a)). The maximum resistance attained is nearly identical for the three

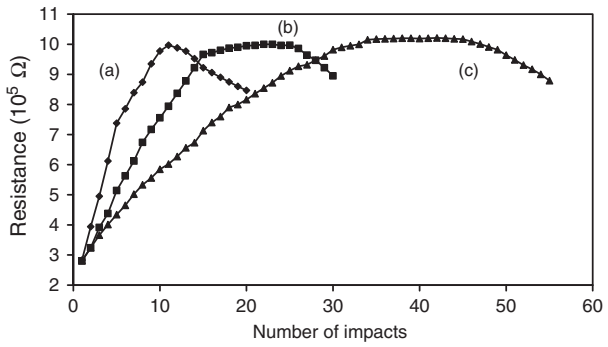

Figure 9. *Surface resistance (Figure 1(a)) upon repeated impact at a fixed energy. The fiber is pitch-based. Impact energy: (a) 2200 J; (b) 1770 J; (c) 1330 J.*

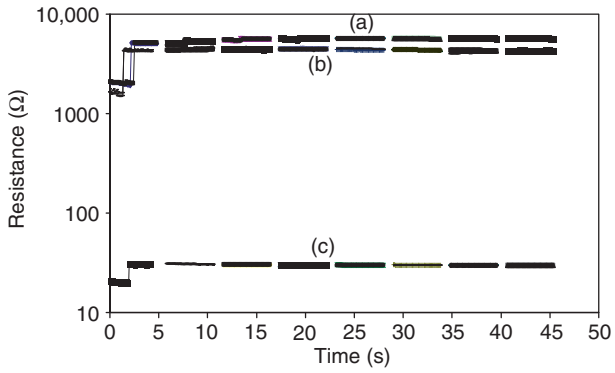

Figure 10. *Surface resistance (Figure 1(a)) upon impact at progressively increasing energy. The impact energy is successively 3990, 3550, 3100, 2660, 2200, 1770, 1330, and 880 J. There are two curves for each specimens: (a) pitch-based fiber; (b) type A PAN-based fiber; (c) type B PAN-based fiber.*

energies, but it is reached at different numbers of impacts for the different energies. Repeated impacts at 2200 J attain a maximum resistance after only 10 impacts, whereas repeated impacts at 1330 J attain the maximum resistance after 35 impacts. The greater is the impact energy, the smaller is the number of impacts needed to inflict damage that is associated with a decrease in resistance.

Sensing Impact at Progressing Decreasing Energy, based on Top Surface Resistance

Figures 5–7 show the sensing of impacts at progressively increasing energy. Figure 10(a) shows the sensing of impacts at progressively decreasing energy for each of the two specimens containing the pitch-based fiber. As shown in Figure 10(a), each impact causes the resistance to increase abruptly, though the effect of an impact diminishes as the energy progressively decreases. The reduction in effect is particularly severe when the energy is reduced from the initial value of 3990 J to the next value of 3550 J. The lower the subsequent impact energy, the less is the incremental increase in resistance upon impact. When the impact energy is reduced to 1770 J, the impact essentially does not affect the resistance any more. Comparison of Figures 5 and 9 show that the impact sensitivity is much better upon increase of the impact energy than upon decrease of the energy, as expected. The fractional increase in resistance is 170% for the total impact sequence (with decreasing energy) relative to the virgin state (Figure 10(a)), whereas it is 200% for the correspondence result obtained with increasing energy (Figure 5(a)).

In case of progressively decreasing energy, the initial impact energy affects the sensitivity of the subsequent impacts at lower energies. A higher initial impact energy results in less ability to detect subsequent low impact energies. For example, with an initial impact energy of 3990 J, subsequent impact below 3400 J cannot be sensed; with an initial impact energy of only 3100 J, subsequent impact as low as 1000 J can be sensed.

Figure 10(b) shows the corresponding results for each of the two specimens containing type A PAN-based fiber. The ability to sense impacts at lower energies after the initial impact at 3990 J is essentially absent. Thus, the type A PAN-based fiber is inferior to the pitch-based fiber for sensing impacts at decreasing energy. The fractional increase in resistance is 160% for the total impact sequence (with decreasing energy) relative to the virgin state.

Figure 10(c) shows the corresponding results for each of the two specimens containing type B PAN-based fiber. The ability to sense impacts at lower energies after the initial impact at 3990 J is essentially absent. In contrast to the other two types of fiber, the type B PAN-based fiber is associated with the resistance decreasing slightly impact-by-impact at progressively decreasing energy. This behavior is attributed to damage that causes increasing chance of fiber–fiber contact. That damage causes the resistance to decrease has been previously reported in carbon fiber (pitch-based) cement paste during cyclic uniaxial tensile or compressive loading (Fu and Chung, 1996). This decreasing trend complicates the interpretation of the resistance in terms of damage. The fractional increase in resistance is 46% for the total impact sequence (with decreasing energy) relative to the virgin state. Thus, at the fiber content of 0.5% by mass of cement, type B PAN-based fiber is inferior to type A PAN-based fiber or the pitch-based fiber for sensing impacts at decreasing energy.

Comparison of Four-probe and Two-probe Methods, based on the Top Surface Resistance

A comparative study is made between the four-probe method (Figure 1(a)) and the two-probe method of surface resistance measurement. Three configurations of the two-probe method are involved (Figure 3).

Table 5 shows the resistance for progressively increasing values of the impact energy. Table 6 shows the

Table 5. DC and AC surface resistances after impact at progressively increasing energy for various contact configurations. The fiber is pitch-based.

	Resistance ($10^3\,\Omega$)							
	Four-probe		Two-probe		Two-probe		Two-probe	
	Figure 1(a) configuration		Figure 3(a) configuration		Figure 3(b) configuration		Figure 3(c) configuration	
Impact energy (J)	DC	AC	DC	AC	DC	AC	DC	AC
0	2.340 ± 0.047	2.013 ± 0.031	2.324 ± 0.035	2.187 ± 0.039	2.545 ± 0.047	2.157 ± 0.061	2.319 ± 0.026	2.218 ± 0.054
880	2.701 ± 0.066	2.572 ± 0.077	2.500 ± 0.071	3.358 ± 0.082	2.759 ± 0.075	2.652 ± 0.087	2.518 ± 0.041	3.468 ± 0.074
1330	3.151 ± 0.057	2.799 ± 0.040	2.671 ± 0.079	2.539 ± 0.091	3.221 ± 0.050	3.125 ± 0.041	3.684 ± 0.028	4.457 ± 0.081
1770	5.133 ± 0.093	4.182 ± 0.154	2.757 ± 0.094	2.601 ± 0.126	3.814 ± 0.105	3.574 ± 0.123	4.763 ± 0.042	5.512 ± 0.074
2200	6.197 ± 0.055	5.218 ± 0.162	2.814 ± 0.114	2.672 ± 0.137	5.463 ± 0.112	5.319 ± 0.098	5.822 ± 0.026	6.688 ± 0.124
2660	7.070 ± 0.058	6.251 ± 0.080	2.829 ± 0.097	2.736 ± 0.188	6.225 ± 0.110	5.921 ± 0.179	6.832 ± 0.071	5.661 ± 0.112
3100	5.763 ± 0.056	4.348 ± 0.059	2.817 ± 0.099	2.674 ± 0.160	5.277 ± 0.111	5.014 ± 0.124	5.825 ± 0.036	4.745 ± 0.110
3550	4.578 ± 0.053	3.172 ± 0.027	2.776 ± 0.073	2.603 ± 0.148	4.328 ± 0.110	4.128 ± 0.129	4.779 ± 0.022	4.575 ± 0.098
3990	3.193 ± 0.063	2.521 ± 0.056	2.717 ± 0.081	2.577 ± 0.099	3.506 ± 0.063	3.246 ± 0.153	4.319 ± 0.034	4.489 ± 0.091

Table 6. Fractional change (relative to the virgin state) of the DC and AC surface resistances due to impact at progressively increasing energy for various contact configurations. The fiber is pitch-based.

	Fractional change in resistance							
	Four-probe		Two-probe		Two-probe		Two-probe	
	Figure 1(a) configuration		Figure 3(a) configuration		Figure 3(b) configuration		Figure 3(c) configuration	
Impact energy (J)	DC	AC	DC	AC	DC	AC	DC	AC
0	0.00	0.00	0.00	0.00	0.00	0.00	0.00	0.00
880	0.15	0.28	0.08	0.54	0.08	0.23	0.09	0.56
1330	0.35	0.39	0.15	0.16	0.27	0.45	0.59	1.01
1770	1.19	1.08	0.19	0.19	0.50	0.66	1.05	1.49
2200	1.65	1.59	0.21	0.22	1.15	1.47	1.51	2.02
2660	2.02	2.11	0.22	0.25	1.45	1.75	1.95	1.55
3100	1.46	1.16	0.21	0.22	1.07	1.32	1.51	1.14
3550	0.96	0.58	0.19	0.19	0.70	0.91	1.06	1.06
3990	0.36	0.25	0.17	0.18	0.38	0.50	0.86	1.02

corresponding fractional change in resistance relative to the state prior to any impact. The fractional change in DC or AC resistance is lower for the two-probe configuration of Figure 3(a) than for the four-probe configuration of Figure 1(a), and the two two-probe configurations of Figure 3(b) and (c), presumably due to the relatively high contact resistance for the two-probe configuration of Figure 3(a).

The AC resistance is lower for the four-probe configuration than any of the three two-probe configurations. This is due to the contact resistance associated with the two-probe method.

The DC resistance prior to any impact is similar for the four-probe method and the two-probe method involving the configurations in Figures 3(a) and (c), but the two-probe method involving the configuration in Figure 3(b) gives slightly higher resistance. This is probably due to the slightly higher degree of polarization for the configuration of Figure 3(b) than that for the configuration of Figure 3(a).

The DC resistance obtained using the configuration of Figure 3(c) prior to any impact is lower than that obtained by using the configuration of Figure 3(b). This is presumably because of the lower contact resistance associated with the configuration of Figure 3(c), due to the large area of the interface between the steel wool and the cement compared to the small area of the interface between the silver paint and the cement. Consistent with this notion is the observation that the fractional change in DC resistance upon impact is higher for the configuration of Figure 3(c) than that of Figure 3(b), as shown in Table 6.

For comparison of AC and DC results upon impact, refer to the section 'Comparison of DC and AC Resistance Results.' Only the DC case is addressed below in relation to comparison among the different contact configurations.

The effect of impact on the resistance differs among the contact configurations, due to the difference in durability of the contacts among the configurations upon impact, as shown in Table 3 and in Figures 5 and 11. The four-probe results (Figure 5(a)) involve the configuration of Figure 1(a)). The two-probe results (Figure 11(a)–(c)) use the configurations of Figure 3(a)–(c), respectively. The resistance measurement is conducted during impact at progressively increasing energy.

With the two-probe method involving any of the three configurations of Figure 3, the resistance increases upon each impact up to an energy of 2660 J, beyond which the resistance decreases upon each impact. The fractional increase in resistance for the end of the impact sequence relative to the virgin state is 21%, 10%, and 54% for Figure 11(a)–(c), respectively. The fractional increase for the highest resistance point in the sequence relative to the virgin state is 22%, 100%, and 180% for Figure 11(a)–(c), respectively. The configuration of Figure 3(a), which involves silver paint line contacts, results in insensitivity to impact beyond 3100 J, Figure 11(a). In spite of the low contact resistance (as indicated by the low value of the measured surface resistance) associated with the silver paint line contacts (Table 5), the degradation of these contacts due to high-energy impacts increases the contact resistance, thus causing the measured two-probe resistance to remain high even after the highest energy impact at 3990 J. In contrast, the two-probe resistance (Figure 11(b) and (c)), obtained using silver paint area contacts or embedded steel contacts decreases substantially upon high-energy impact, due to relatively little degradation of the contacts at high impact energies. The four-probe resistance (Figure 5(a)), as obtained using silver paint line contacts, is similar in behavior to the two-probe resistance obtained using silver paint area contacts or embedded steel contacts, because the four-probe method is quite insensitive to the contact degradation.

The tendency for the resistance to decrease with time before and after an impact (not during the impact) is greater for the two-probe method using silver paint area contacts than that using embedded steel contacts, as shown by comparing Figure 11(b) and (c). Both, two-probe configurations with silver paint area contacts and embedded steel contacts, give lower noise in the resistance data than the two-probe configuration with silver paint line contacts. Among the three two-probe configurations in Figure 3, the configuration in Figure 3(c), which involves embedded steel contacts, is most effective. The two-probe configuration in Figure 3(b), which involves silver paint area contacts, is almost as effective. However, the two-probe configuration in Figure 3(a), which involves silver paint line contacts, is much less effective.

For the four-probe method (Figure 5(a)), the fractional increase in resistance is 33% for the end of the sequence relative to the virgin state, and is 200% for the highest resistance point in the sequence relative to the virgin state. This means that the four-probe method involving silver paint line contacts is comparable in effectiveness to the two-probe method involving silver paint area contacts.

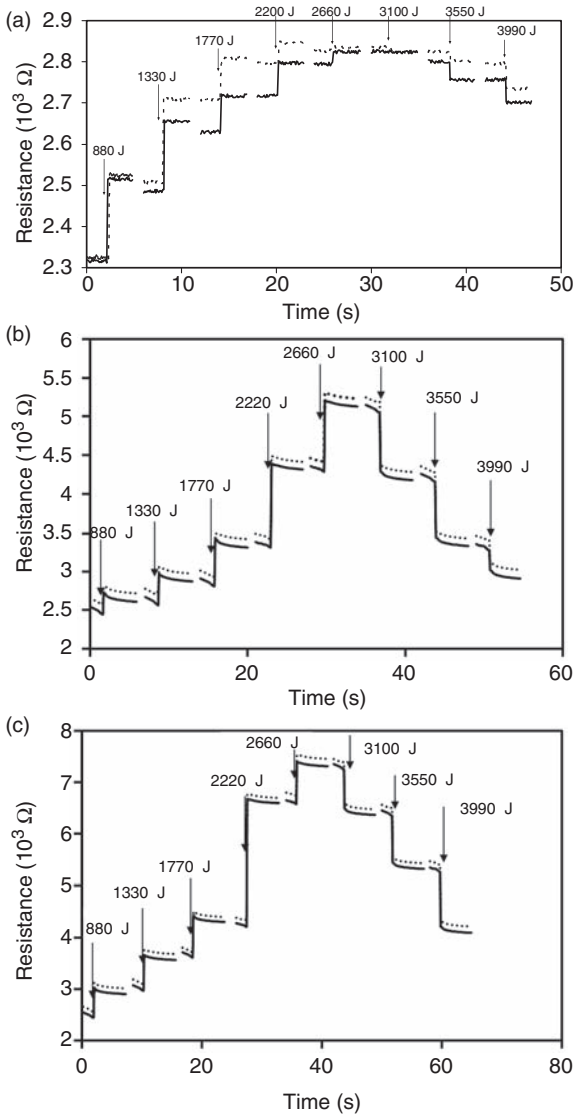

Figure 11. *Two-probe surface resistance (Figure 3) upon impact at progressively increasing energy. The impact energy is successively 880, 1330, 1770, 2200, 2660, 3100, 3550, and 3990 J. The two curves are for two specimens, each containing the pitch-based carbon fiber: (a) configuration of Figure 3(a); (b) configuration of Figure 3(b); (c) configuration of Figure 3(c).*

Figure 12(a) shows corresponding results for type A PAN-based fiber, using the two-probe configuration of Figure 3(b). The behavior is similar to that of the pitch-based fiber shown in Figure 11(b), though the fractional decrease in resistance upon impact in the high-energy regime is lower. This suggests that two-probe silver paint area contact resistance contribution to the measured resistance is higher for type A PAN-based fiber than the pitch-based fiber. This difference may be

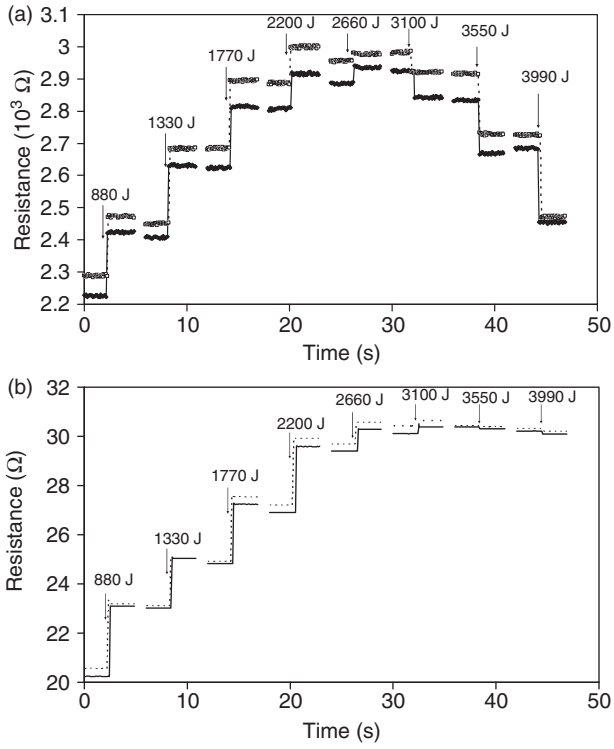

Figure 12. *Two-probe surface resistance (Figure 3(c)) upon impact at progressively increasing energy. The impact energy is successively 880, 1330, 1770, 2200, 2660, 3100, 3550, and 3990 J. The two curves in each graph are for two specimens: (a) type A PAN-based fiber; (b) type B PAN-based fiber.*

due to the difference in the extent of contact between fiber and silver paint area contacts for the two types of fiber. A greater extent of contact between fiber and the electrical contact material will result in a lower contact resistance (Chen and Chung, 1993a,b, 1995).

Figure 12(b) shows the corresponding results for type B PAN-based fiber, using the two-probe configuration of Figure 3(c). Both the resistance and the fractional change in resistance are similar to those of the four-probe results for the same fiber (Figure 7(a)). The resistance stays high in the high-energy regime for both two-probe and four-probe results.

Comparison of the two-probe and four-probe results for all three fiber types shows that the most effective sensing is provided by the pitch-based fiber in combination with the four-probe method (Figure 5(a)). The two-probe method is simpler to implement than the four-probe method, but it is not very effective in the high-energy regime (above 3100 J) and the fractional change in resistance due to impact is low (Figure 11).

Sensing Impacts at Progressively Increasing Energy, based on the Longitudinal Volume Resistivity

Figure 13(a) shows the results for the longitudinal volume resistivity during impact at progressively increasing energy for each of two specimens containing

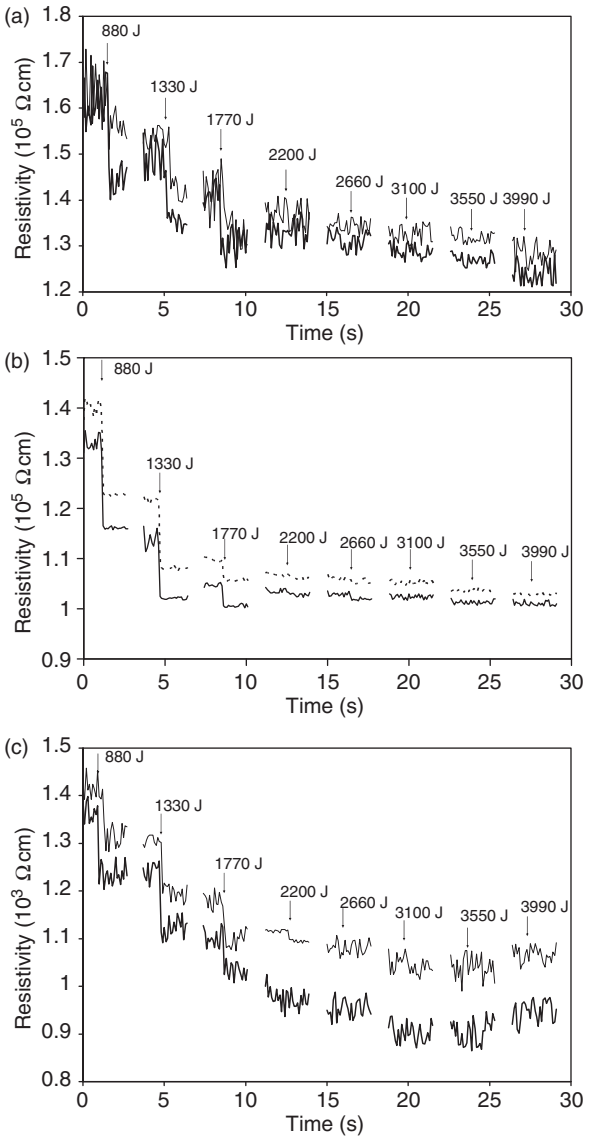

Figure 13. *Longitudinal volume resistivity (Figure 1(c)) upon impact at progressively increasing energy. The two curves in each graph are for two specimens. The impact energy is successively 880, 1330, 1770, 2200, 2660, 3100, 3550, and 3990 J: (a) pitch-based fiber; (b) type A PAN-based fiber; (c) type B PAN-based fiber.*

the pitch-based fiber. The resistivity shown is obtained from the measured resistance (around $2.5 \times 10^3\ \Omega$ for the virgin state) and the specimen dimensions. It decreases monotonically as the impact energy is increased, although the data are noisy and the decrease is observable only for impact energies of 1770 J and below. The fractional decrease in resistivity up to the highest energy of 3990 J is 22%. This trend is attributed to damage that causes increasing chance of fiber–fiber contact (Fu and Chung, 1996). Due to the noisiness and the small effect of impact on the resistivity, the longitudinal volume resistance is not a good indicator of impact damage.

Figure 13(b) shows the corresponding results for type A PAN-based fiber. The results are similar to those for

the pitch-based fiber (Figure 13(a)), though the data are less noisy. The fractional decrease in resistivity up to the highest energy of 3990 J is 20%.

Figure 13(c) shows the corresponding results for type B PAN-based fiber. The results are similar to those of the other two fiber types, though the resistance slightly increases at impact energy of 3550 J and above. The fractional decrease in resistivity is 34% up to 3100 J and is 31% up to 3990 J. These values are higher than those for the other two types of fiber.

Sensing Repeated Impacts at a Fixed Energy, based on the Longitudinal Volume Resistivity

Figure 14 shows the monotonic decrease in longitudinal volume resistivity (Figure 1(c)) for each of three specimens (with pitch-based carbon fiber) impacted at a fixed energy of 3990 J. This trend is consistent with that obtained upon progressively increasing impact energy (Figure 13(a)). The fractional decrease in resistivity is 29% over the total of 12 impacts.

Sensing Repeated Impacts at a Fixed Energy, based on the Oblique Resistance

The oblique resistance is measured using the configuration of Figure 1(b). It is higher than the surface resistance (Table 4), due to the larger distance between the voltage contacts for the former.

Figure 15 shows the oblique resistance at progressively increasing impact energy for each of the two specimens with pitch-based carbon fiber. Impact at any of the energies does not affect the oblique resistance, indicating absence of impact damage sensitivity. The sensitivity is inferior to both the longitudinal volume resistance (Figure 13(a)) and the surface resistance (Figure 5(a)). The insensitivity of the oblique resistance is partly because of the poor sensitivity of the oblique resistance to surface damage, and partly because of the small sensed volume compared to that for the longitudinal volume resistance. The current path is throughout the whole cross-section of the specimen for the longitudinal volume resistance (Figure 1(c)), but is between the two voltage contacts on the two opposite surfaces of the specimens for the oblique resistance (Figure 1(b)).

The oblique resistance decreases with time, both before and after an impact at, and energy of 2660 J or above (Figure 15). This decreasing trend is attributed to resistance heating associated with the oblique current. Although the surface resistance is lower than the oblique resistance (Table 4), heating associated with the surface current is less than that associated with the oblique current, due to the heat dissipation from the surface to the environment, thus causing a weaker decreasing trend for the surface resistance (Figure 5(b)).

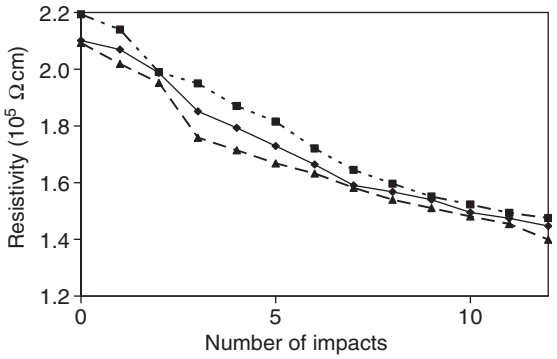

Figure 14. *Longitudinal volume resistivity upon impact at a fixed energy of 2660 J. The three curves are for three specimens. The fiber is pitch-based.*

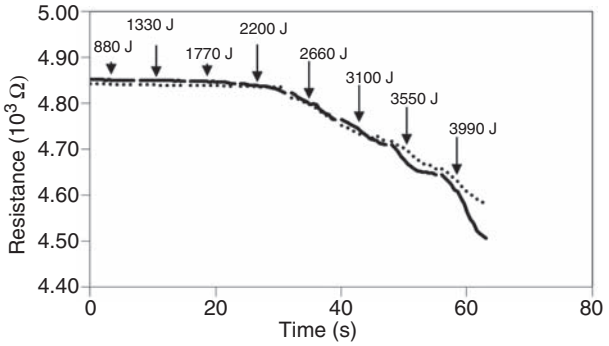

Figure 15. *Oblique resistance (Figure 1(b)) upon impact at progressively increasing energy. The two curves are for two specimens. The fiber is pitch-based.*

Sensing of Impact Outside the Region of Resistance Measurement, based on the Surface Resistance and the Oblique Resistance

Using the surface resistance measurement configuration in Figure 2, the sensing of impact outside the region of resistance measurement is assessed. In Figure 2, the impact is just outside this region, which is the region bound by the voltage contacts.

Impact outside the region of resistance measurement does not cause any change in the measured surface resistance. The insensitivity occurs even when the carbon fiber content is increased from 0.5% to 1.0% and 1.5% by mass of cement. Increase of the fiber content decreases the surface resistance, as shown in Table 4.

Similar impact just outside the region of oblique resistance measurement shows similar insensitivity at these fiber contents. Similar impact just outside the region of longitudinal volume resistance also indicates insensitivity, as shown upon impact at progressively increasing energy for the various fiber contents. Increase of the fiber content decreases the longitudinal volume resistivity, as shown in Table 4.

The negative result means that the self-sensing is feasible only when the resistance is measured for a part of the specimen that contains the point of impact.

In contrast, self-sensing by resistance measurement is feasible for segments that do not include the point of maximum deflection in three-point flexural loading (Wen and Chung, 2006b). Thus, the negative result is attributed to the localized nature of the damage resulting from impact. In contrast, damage resulting from flexure is spread out.

Carbon Fiber Mortar as a Coating for Sensing

The use of carbon fiber mortar as a coating rather than a monolithic block facilitates implementation of the sensing technology in existing structures. Thus, carbon fiber mortar of various thicknesses is applied as a coating on plain mortar and the surface resistance is measured during impact at 3550 J. As shown in Figure 16(a), the resistance decreases with increasing coating thickness. This is due to the penetration of the current to depths below the surface. The effect of impact on the resistance is absent when the thickness is 1.0 mm or below. The sensitivity increases with increasing thickness from 2.0 to 5.0 mm. The sensitivity is similar for thicknesses of 5.0 and 10.0 mm.

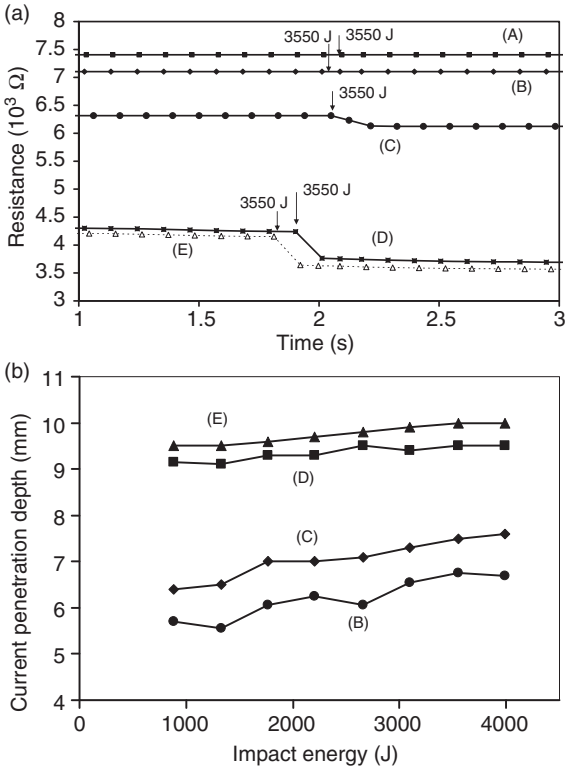

Figure 16. *(a) Surface resistance (Figure 1(a)) upon impact at progressively increasing energy. The impacted surface is a pitch-based carbon fiber mortar coating on a plain mortar substrate. The coating thickness (u) is (A) 0.25 mm, (B) 1.0 mm, (C) 2.5 mm, (D) 5.0 mm, and (E) 10.0 mm. (b) The calculated current penetration depth versus the impact energy, as calculated based on the changes in resistance in (a).*

The feasibility of a carbon fiber mortar layer to sense damage means that it is not necessary for the entire structure to contain carbon fiber. Moreover, the coating may be applied to existing structures.

The depth of current penetration can be estimated from the effect of the coating thickness on the measured surface resistance. Consider that the current penetration is for a depth of $u+q$, where u is the coating thickness and q is the depth of penetration into the plain mortar substrate. In case that the current does not penetrate the coating completely, q is negative. The measured surface resistance R consists of the volume resistance of the coating (R_c) and that of the part of the substrate to which current has penetrated (R_s), such that the two resistances are in parallel.The bulk values of ρ_c and ρ_s are within a factor of 4 (Table 4). For simplicity, their difference is ignored in the estimation of the effect of current penetration on the measured surface resistance R. Hence:

$$\log R = -A \log (u+q), \tag{1}$$

where A is a parameter that depends on the resistivity and the dimensions. By using q as an adjustable parameter for each coating thickness, with the adjustment aimed at achieving a straight line of negative slope for the data plotted in the form of log R versus $\log(u+q)$, the value of q is obtained for each coating thickness and each state of damage. The current penetration depth is $u+q$. The results are shown in Table 7. The largest depth of current penetration is 10 mm, as obtained for the case of the 10 mm coating thickness.

Effect of Carbon Fiber Content

Increase in the carbon fiber content monotonically decreases the resistance or resistivity. It is shown in Table 4 for the surface resistance, oblique resistance and longitudinal volume resistivity.

The carbon fiber content also affects the impact damage sensing effectiveness, as shown in Figure 17(a), for the surface resistance measured at progressively increasing impact energy using the configuration of Figure 1(a). In the absence of carbon fiber, the sensing ability is absent. The sensitivity is highest at fiber

Table 7. Current penetration depth u + q, where u is the pitch-based carbon fiber mortar coating thickness and q is the depth of penetration into the plain mortar substrate.

u (mm)	*q* (mm)	*u* + *q* (mm)	*R* (Ohm)
0.25	5.8	6.05	7100
2.5	4.3	6.8	6300
5	4.5	9.5	4400
10	0	10	4250

contents of 0.5% and 1.0% by mass of cement, as shown by the values of the fractional change in resistance relative to the virgin state in Figure 17(b). Although these two fiber contents give similar values of the factional change in resistance, the higher resistance for the lower fiber content makes the resistance change easier to detect. Increasing the fiber content to 1.5% by mass of cement degrades the sensing ability from that at 1.0% by mass of cement, as expected from the fact that the percolation threshold (between 0.5% and 1.0%, Chen and Chung, 1995) is exceeded in the case of 1.5%.

In spite of the decrease in the volume electrical resistivity of the mortar as the carbon fiber content increases (Table 4), the sensing ability, as shown by the fractional change in resistance due to the impact damage (Figure 17(b)), is not enhanced by increase in fiber content beyond 0.50% by mass of cement. This is consistent with previous sensing results obtained during uniaxial compression (Chen and Chung, 1996). Since carbon fibers are expensive compared to cement, a low fiber content of 0.5% by mass of cement is recommended.

That the damage sensitivity of carbon fiber mortar is highest at an intermediate fiber content of 0.50–1.00% by mass of cement (i.e., 0.24–0.48 vol.%) is consistent with previous report that the strain sensitivity (ability to sense strain rather than damage through resistance measurement) of carbon fiber reinforced cement is higher at an intermediate fiber content of 1.00% by mass of cement (i.e., 0.95 vol.%) than fiber contents of 0.50% or 1.50% by mass of cement (0.48 or 1.43 vol.%, respectively) (Wen and Chung, 2005). Furthermore, that the damage sensitivity of carbon fiber mortar is similar for 0.50% and 1.00% by mass of cement (i.e., 0.24% and 0.48 vol.%) is consistent with prior report that the strain sensitivity of carbon fiber reinforced cement is quite close for 0.50% and 1.00% by mass of cement (i.e., 0.48 and 0.95 vol.%) (Wen and Chung, 2005).

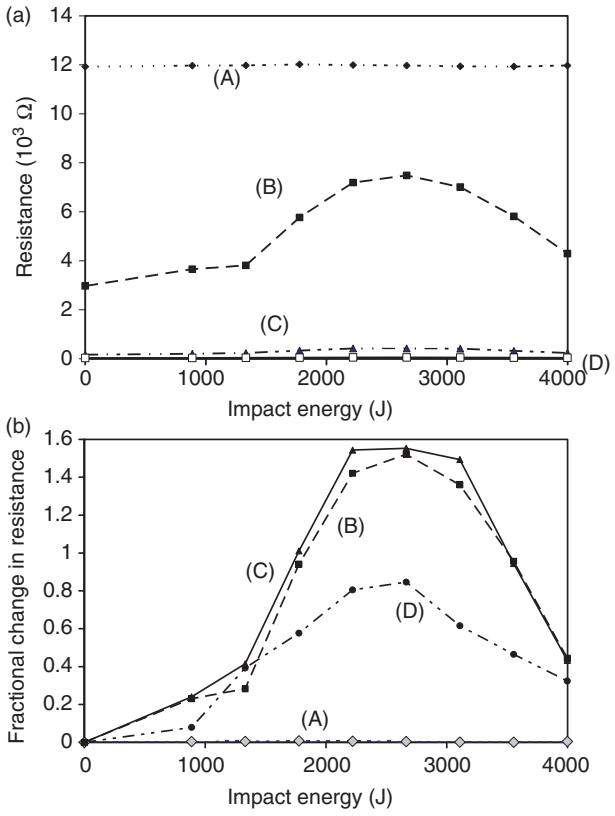

Figure 17. *Surface resistance (Figure 1(a)) upon impact at progressively increasing energy. Each curve is for a given proportion (by mass of cement) of pitch-based carbon fiber. Specimen (A) contains 0.0%, (B) contains 0.5%, (C) contains 1.0%, and (D) contains 1.5%. (b) shows the corresponding fractional change in resistance (relative to the value prior to any impact) for these specimens.*

The results in this section are consistent with those in the section'Sensing Impact at Progressing Increasing Energy, based on the Top Surface Resistance,' which compares the sensing performance for three types of fibers at the same content of 0.5% by mass of cement. The results of these two sections imply the following. For effective sensing, the carbon fiber can be made from pitch or PAN, provided that the resistivity of the mortar is in the range 104–105 Ω cm (Section 'Sensing Impacts at Progressively Increasing Energy, based on the Longitudinal Volume Resistivity'), as attained by pitch-based carbon fiber (15 μm diameter, 5 mm long, unsized) at 0.5% or 1.0% by mass of cement or by type A PAN-based carbon fiber (7 μm diameter, 8 mm long, desized) at 0.5% by mass of cement. Due to the low mortar resistivity of 103 Ω cm (Table 4 and Section 'Sensing Impacts at Progressively Increasing Energy, based on the Longitudinal Volume Resistivity'), pitch-based carbon fiber at 1.5% by mass of cement and type B PAN-based carbon fiber (7 μm diameter, 8 mm long, unsized) at 0.5% by mass of cement are less effective. In the absence of fiber, there is no sensing ability.

Comparison of DC and AC Resistance Results

AC resistance is advantageous over DC resistance in that its measurement does not cause polarization, whereas DC resistance measurement can be accompanied by polarization. Polarization stems from the dielectric part of the electrical behavior. The polarization causes the measured resistance to increase beyond the true value (Cao and Chung, 2004; Wen and Chung, 2001c). However, DC measurement involves simpler instrumentation than AC measurement.

Figure 18 and Table 5 show comparison of DC and AC surface resistances, as measured at progressively increasing impact energy using the configuration of Figure 1(a). Table 6 shows the corresponding fractional change in resistance relative to the virgin state. The DC and AC results are similar for all the impact energies as shown in Figure 18(a), although the AC resistance is lower than the DC resistance (Table 5). For the three

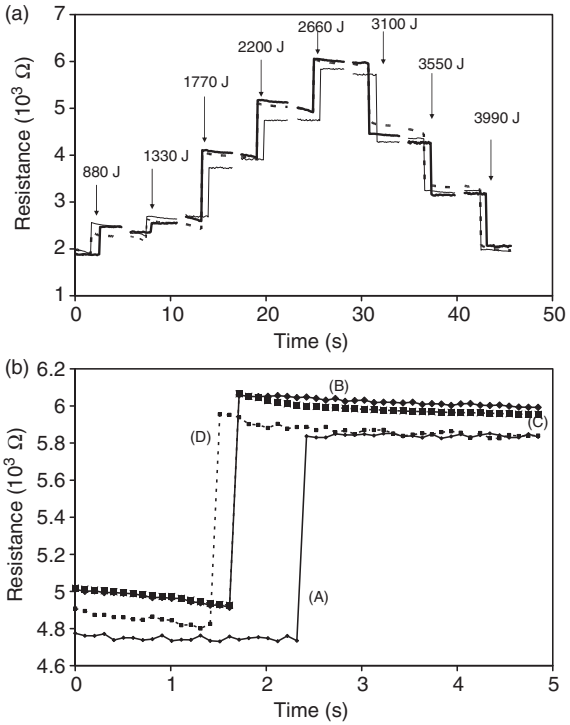

Figure 18. *(a) Surface resistance upon impact at progressively increasing energy. The impact energy is successively 880, 1330, 1770, 2200, 2660, 3100, 3550, and 3990 J. Two solid curves: AC; dashed curve: DC.(b) A magnified view of the effect of the 2660 J impact. (A) and (B) are two specimens measured under AC. (C) and (D) are two specimens measured under DC.*

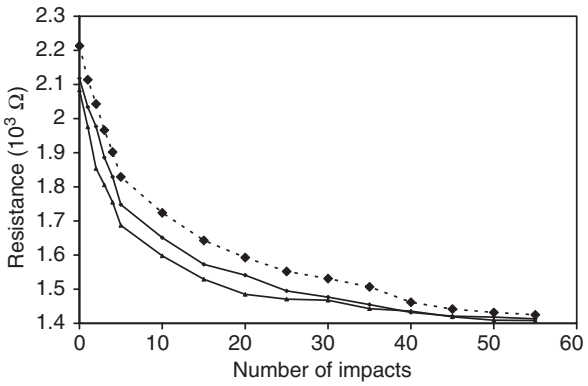

Figure 19. *Surface resistance (Figure 1(a)) upon repeated impact at 3990 J. The fiber is pitch-based. The dotted curve is for DC; the solid curves are for two specimens measured under AC.*

two-probe configurations, the fractional change in AC resistance tends to be slightly higher than the fractional change in DC resistance, both relative to the virgin state. This difference between AC and DC results may be due to the polarization that occurs during DC measurement and the increase in measured (apparent) DC resistance due to polarization (Wen and Chung, 2001c; Cao and Chung, 2004). Due to the polarization effect, the effect of the contact resistance on the measured resistance, as shown by comparing the four-probe and two-probe methods is observed less clearly under DC than AC.

Table 8. Surface resistance (A) (Figure 1(a)) and longitudinal volume resistivity (B, C) upon repeated impact at 3990 J. The fiber is pitch-based. The distance between the voltage contacts is 51 mm (Figure 4(a)) in B, and 203 mm (Figure 4(b)) in C. The bold numbers indicate the specimen number.

	Resistance (10^3 Ω)			Resistivity (10^5 Ω cm)				
	(A)			(B)			(C)	
Impact no.	1†	2†	3*	1*	2†	3†	1*	2†
0	2.118	2.084	2.213	2.101	2.125	2.168	2.236	2.225
1	2.034	1.976	2.114	2.070	2.100	2.079	2.191	2.185
2	1.977	1.854	2.043	1.996	2.054	1.965	2.125	2.115
3	1.886	1.806	1.966	1.952	1.986	1.936	2.053	2.081
4	1.829	1.755	1.902					
5	1.748	1.687	1.829	1.890	1.879	1.869	2.005	1.990
7				1.791	1.783	1.795	1.963	1.905
10	1.651	1.598	1.724	1.715	1.763	1.735	1.915	1.896
12				1.687	1.666	1.679	1.825	1.831
15	1.573	1.529	1.643					
20	1.541	1.485	1.593					
25	1.495	1.471	1.552					
30	1.477	1.468	1.531					
35	1.455	1.443	1.507					
40	1.432	1.436	1.462					
45	1.421	1.419	1.442					
50	1.418	1.409	1.432					
55	1.413	1.408	1.425					

*DC.
†AC

Figure 19 and Table 8 shows that AC and DC surface measurements give similar results for the multiple impacts at the same energy of 3990 J for each of three specimens. Table 8 also shows a similarity of the AC and DC results for the longitudinal volume resistivity, as measured using the specimen configurations of Figure 4(a) and (b), respectively.

Effect of Length of Resistance Measurement Region

A longer length of the region of resistance measurement facilitates sensing large regions of a structure. Since the damage is localized, the impact damage sensitivity is expected to decrease with increasing length of the resistance measurement region, i.e., increasing distance between the voltage contacts. The effect of this length is investigated by measuring the longitudinal volume resistivity, using the configurations of Figure 1(c) (with this length being 25 mm), Figure 4(a) (with this length being 51 mm) and Figure 4(b) (with this length being 203 mm). The results are shown in Figures 14, 20(a), and (b) for lengths 25, 51, and 203 mm, respectively. The fractional decrease in resistivity after the sequence of impacts at a fixed energy of 3990 J is 36%, 21%, and 18% for Figures 14, 20(a), and (b), respectively. This means that the impact damage sensitivity indeed decreases with increasing length of the region of resistance

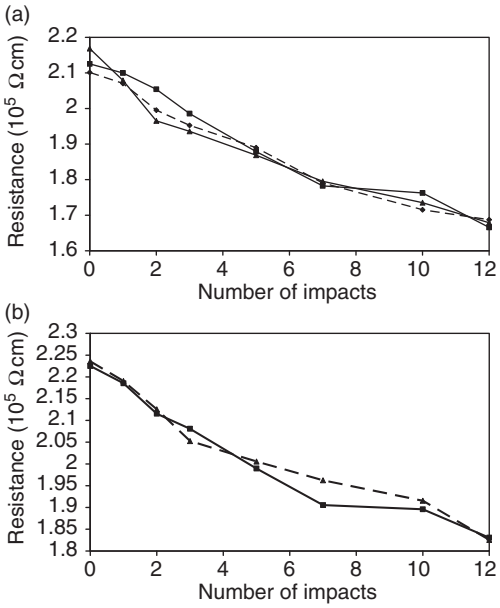

Figure 20. *Longitudinal volume resistivity upon repeated impact at a fixed energy of 3990 J. The multiple curves in a graph are for different specimens. The fiber is pitch-based. The distance between the voltage contacts is relatively large, namely (a) 51 mm (Figure 4(a)); (b) 203 mm (Figure 4(b)).*

measurement. The effect of length is larger for length below 51 mm than length above 51 mm. Nevertheless, the sensitivity is adequate at the largest distance of 203 mm (Figure 20(b)). Based on geometric consideration, the fractional decrease in resistivity after impact should be inversely proportional to the length of the region of resistance measurement. However, the inverse proportionality is not supported by the data. In other words, the decrease in sensitivity with increasing length is less than that expected based on geometry. The cause for this is unclear, but this is advantageous for practical sensing of large regions.

Effect of Impact Damage on the Flexural Properties

Figure 21 and Table 9 show that the flexural strength and toughness are decreased by impact, such that their values decrease monotonically with increasing maximum impact energy. After impact at 1330 J, the flexural strength is decreased by about 23%, while the flexural toughness is decreased by about 56%. This amount of damage is essentially not visible on the surface, but it can be clearly sensed, as shown in Figure 5(a). After cumulative impacts from the virgin state to 3990 J, using the sequence of impact energy shown in Table 3, the overall decrease in flexural strength is 78% and the overall decrease in flexural toughness is 89%, as shown in Table 9, which also shows that the maximum deflection (which relates to the ductility) is also reduced by the impact damage. Impact at 3990 J causes fracture in some

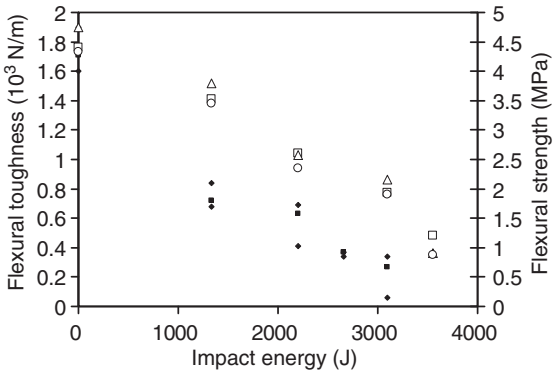

Figure 21. *Residual flexural properties for various impact energies, each of which being the maximum energy in the progression. The fiber is pitch-based. Residual flexural toughness is shown by solid symbols. Residual flexural strength is shown by open symbols.*

of the specimens, so that flexural testing becomes impossible for these specimens.

The largest fractional change in resistance in Table 4 is obtained after impact at 2660 J using the four-probe configuration (Figure 1(a)) under AC condition. The 2660 J impact corresponds to a decrease in flexural strength of 55% and decrease in flexural toughness of 79%.

Table 9 shows that, both before and after impact at any of the energies, the pitch-based carbon fiber gives higher flexural strength than the type A PAN-based carbon fiber, but the type B PAN-based fiber gives the highest flexural strength among the three types of fiber. The superiority of the type B PAN-based fiber as a reinforcement is consistent with the fact that this type of fiber gives the lower resistance or resistivity (Figure 7 compared to Figures 5 and 6). The superiority of both mechanical and electrical properties of the type B PAN-based fiber is probably due to a higher degree of fiber dispersion, which is sensitive to the surface condition of the fiber. On the other hand, among the three types of carbon fiber, the type B fiber is least effective for self-sensing (Section 'Sensing Impact at Progressing Increasing Energy, based on the Top Surface Resistance'), due to the low resistivity of the type B fiber specimens.

Correlation of Surface Resistance and Residual Flexural Strength

Figure 22 shows correlation between the top surface resistance and the flexural strength after impact at various energies. There is a monotonic relationship between these attributes in the regime in which the resistance increases upon impact (Figure 5(a)). As the impact energy increases, the resistance increases, and the flexural strength decreases. This correlation allows the resistance to be an indicator of the cumulative damage. However, it is not valid only in the regime in which the resistance decreases upon impact (Figure 5(a)).

Table 9. Flexural properties of pitch-based carbon fiber specimens after impact at various maximum impact energies. The maximum energy is the highest energy used in a sequence of progressively increasing energy. The maximum deflection is the midspan deflection when the flexural stress has been reduced to 0.15 MPa (10 lb load). The progression of impact energy is shown in Table 3. Specimens with the same type of fiber but used for different impact energies are different.

Impact energy (J)	Carbon fiber type	Flexural strength (MPa)	Maximum deflection (mm)	Flexural toughness (10^3 N/m)
0	Pitch-based	4.41 ± 0.41	1.38 ± 0.68	1.91 ± 0.28
	Type A PAN-based	4.27 ± 0.53	1.46 ± 0.53	1.89 ± 0.27
	Type B PAN-based	4.83 ± 0.46	1.71 ± 0.56	2.02 ± 0.31
1330	Pitch-based	3.53 ± 0.33	1.05 ± 0.77	0.68 ± 0.16
	Type A PAN-based	3.37 ± 0.43	0.78 ± 0.69	0.69 ± 0.39
	Type B PAN-based	4.28 ± 0.50	0.93 ± 0.62	0.77 ± 0.26
2200	Pitch-based	2.60 ± 0.25	1.21 ± 0.40	0.41 ± 0.28
	Type A PAN-based	2.43 ± 0.38	1.33 ± 0.64	0.40 ± 0.32
	Type B PAN-based	3.26 ± 0.37	1.50 ± 0.71	0.49 ± 0.34
2660	Pitch-based	1.94 ± 0.25	0.81 ± 0.13	0.37 ± 0.03
	Type A PAN-based	1.79 ± 0.32	0.93 ± 0.42	0.35 ± 0.25
	Type B PAN-based	2.71 ± 0.49	1.10 ± 0.36	0.48 ± 0.27
3100	Pitch-based	1.21 ± 0.33	0.68 ± 0.10	0.06 ± 0.28
	Type A PAN-based	1.09 ± 0.84	0.77 ± 0.35	0.08 ± 0.49
	Type B PAN-based	1.87 ± 0.56	0.96 ± 0.38	0.15 ± 0.36

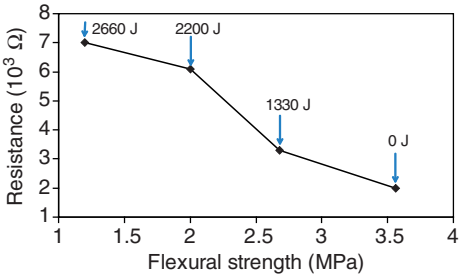

Figure 22. *Correlation of the surface resistance (Figure 5(a)) and the residual flexural strength for various impact energies, each of which being the maximum energy in the progression. The fiber is pitch-based.*

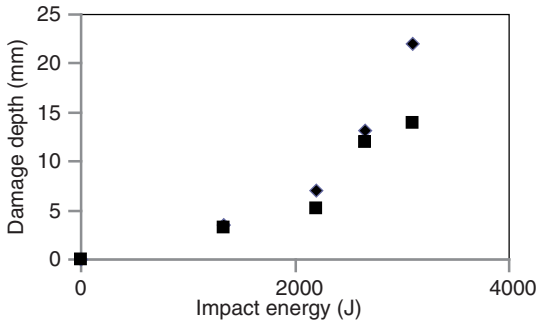

Figure 23. *Damage depth calculated from the residual flexural strength results in Figure 22. The fiber is pitch-based. The two symbols are data for two different specimens.*

Based on the relationship between the flexural stress and the specimen thickness:

$$\frac{\text{Residual flexural strength}}{\text{Original flexural strength}} = \left(\frac{\text{Residual thickness}}{\text{Original thickness}}\right)^2, \tag{2}$$

where the residual thickness refers to the effective thickness after damage and is given by:

$$\text{Residual thickness} = \text{Original thickness} - \text{Damage depth}. \tag{3}$$

The damage depth includes the indent depth, which is negligibly small compared to the damage depth. To illustrate this calculation, the 2660 J impact is considered for the case of the pitch-based carbon fiber. The residual flexural strength is 1.94 MPa, and the original flexural strength of 4.41 MPa (Table 9). This gives a residual thickness of 27 mm, and hence a damage depth of 13 (i.e., 40–27) mm. Figure 23 shows the calculated damage depth for various impact energies in the regime in which the resistance increases upon impact for the case of the pitch-based carbon fiber.

The current penetration depth is 10 mm (Section 'Carbon Fiber Mortar as a Coating for Sensing'). The depth of current penetration is less than but close to the damage depth of 13 mm for the 2660 J impact. This means that most of the damaged region is detected electrically.

Assuming that the entire damage depth is sensed electrically and that the area of damage is the area of the indent, a simple calculation involving electrical resistances in series and in parallel shows that the volume resistivity of the damaged region (not the entire region of resistance measurement) is $3.1 \times 10^6\,\Omega\,\text{cm}$ after the 2660 J impact shown in Figure 5(a), compared to the value of $1.6 \times 10^5\,\Omega\,\text{cm}$ prior to any impact (Figure 13(a)). Figure 24 shows the calculated volume

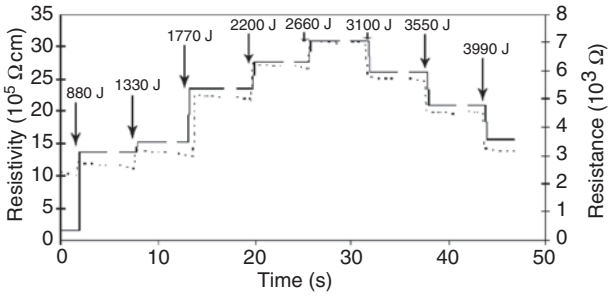

Figure 24. *The calculated volume resistivity of the damaged region (solid curve) and the measured surface resistance (dashed curve, Figure 5(a)), each varying with the progressively increasing impact energy for the case of the pitch-based carbon fiber.*

resistivity of the damaged region as a function of the progressively increasing impact energy, based on the measured surface resistance for the case of the pitch-based carbon fiber (Figure 5(a)). Also shown in Figure 24 is the measured surface resistance. The calculated resistivity of the damaged region and the measured surface resistance vary with the impact energy similarly.

Effect of Impact Damage on the Morphology

Figure 25 shows optical photographs obtained for the same specimen after impact at progressively increasing energy. Figures 25(a) (2660 J) and Figure 25(b) (3550 J) show slight surface indentation without cracking, but Figure 25(c) (4440 J) shows cracking. Scanning electron microscopy did not give additional information. The 2660 J impact, for example, corresponds to a decrease in flexural strength of 55% and decrease in flexural toughness of 79%, Section 'Correlation of Surface Resistance and Residual Flexural Strength'). Figure 25(a) shows that this level of damage does not cause any cracking, but it leaves a shallow indent at the impact location.

FURTHER DISCUSSION

Major damage that is accompanied by irreversible strain causes the volume resistivity of carbon fiber reinforced cement to increase irreversibly (Wen and Chung, 2006c). Thus, major damage is expected to cause both the surface resistance and the volume resistivity to increase, whether cracking is involved with the major damage or not.

The sensing ability described in this article is limited to the carbon fiber cement-based mortar. The method is not for sensing damage in the steel reinforcement or that at the steel-concrete interface. For steel-concrete interface monitoring, the contact resistance of this interface may be measured (Cao and Chung, 2001).

For all of the impacts up to the highest energy of 3990 J (Figure 5(a)), there is no cracking, but the surface resistance effect of impact is substantial.

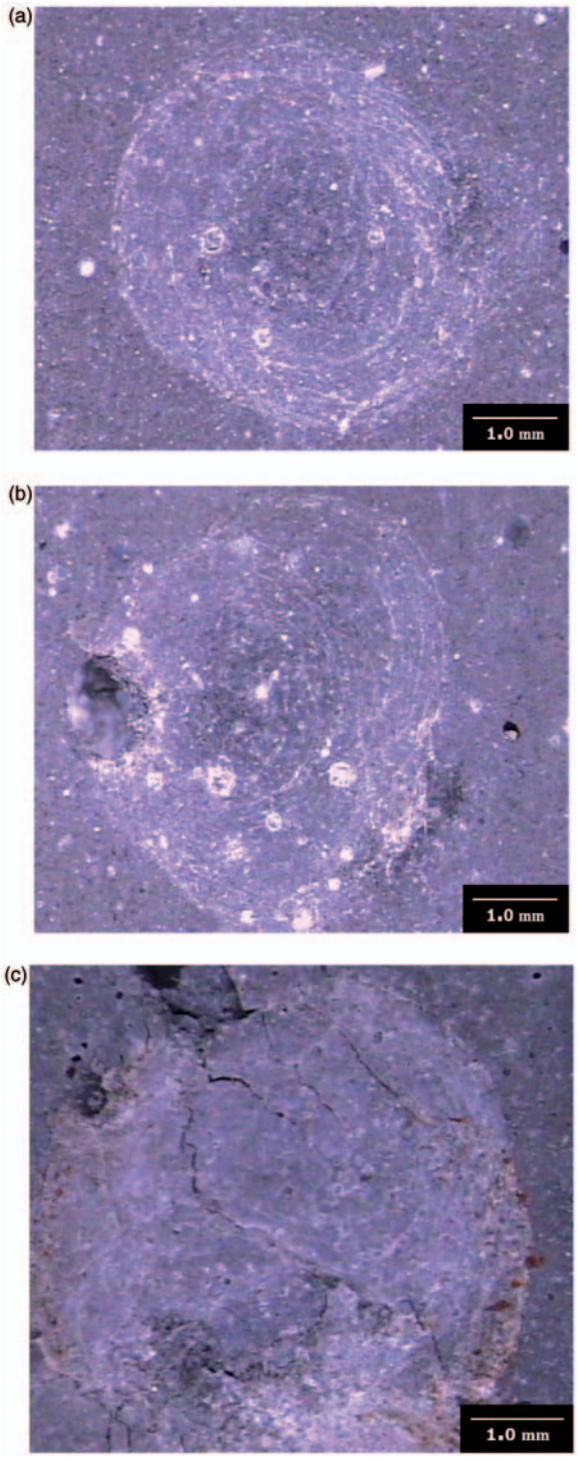

Figure 25. *Optical photographs of the same pitch-based carbon fiber mortar specimen after impact at progressively increasing energy. (a) 880, 1330, 1770, 2200 and 2660 J in the progression; (b) 3100 and 3550 J after the progression in (a); (c) 3990 and 4440 J after the progression in (b).*

The surface resistance increases upon impact up to 2660 J, but decreases upon impact at 3100 J and above (Figure 5(a)). However, the longitudinal volume resistivity decreases upon impact, particularly in the low-energy

regime (Figure 13(a)). For materials in general, damage typically causes the resistance to increase, due to the high resistance associated with defects. Thus, the increase of the surface resistance upon impact up to 2660 J is consistent with the usual expectation. The change from the behavior of the surface resistance increasing upon impact in the low-energy regime to that of the surface resistance decreasing upon impact in the high-energy regime is attributed to the change from superficial damage (i.e., damage of the near surface region only) to deeper minor damage that increases the extent of contact between adjacent fibers. The longitudinal volume resistivity decreases upon damage because of interior minor damage associated with the increase in the extent of contact between fibers. The minor damage that causes the resistance to decrease can occur in the absence of cracking, as it just involves damage of the cement matrix between adjacent fibers. Such damage has been previously observed during fatigue of carbon fiber (pitch-based) reinforced cement mortar (Fu and Chung, 1996). This localized damage may be due to the slight pull-out or push-in of crack-bridging fibers during impact. Whether a fiber undergoes pull-out or push-in depends on its orientation relative to the direction of impact.

The volume resistivity decreases (Figure 13(a)) while the surface resistance increases (Figure 5(a)) in the low-energy regime. This is because minor interior damage accompanies the superficial damage in the low-energy regime and the volume resistivity is sensitive to even minor interior damage, though it is insufficiently sensitive to superficial damage. On the other hand, the surface resistance is highly sensitive to the superficial damage.

The volume resistivity does not change upon impact in the high-energy regime (Figure 13(a)). This is attributed to the combined effect of: (i) the minor interior damage that causes the increased contact between adjacent fibers (Fu and Chung, 1996), and (ii) the major damage that causes the resistivity to increase (Wen and Chung, 2006c).

The oblique resistance is insensitive to impact damage (Figure 15), due to the low sensitivity to both surface damage and interior damage. The poor sensitivity to interior damage is because of the small sensed volume. The sensed volume is much larger for the longitudinal volume resistivity. On the other hand, the oblique resistance is sensitive to flexural damage under three-point bending (Wen and Chung, 2006b). Flexural damage differs from impact damage in that it is spatially spread out, in contrast to the localized nature of impact damage. Due to the spread-out nature of flexural damage, the chance of the oblique current path to intersect an area of damage is high. Due to the localized nature of impact damage, the change of the oblique current path to interact an area of damage is low.

As shown in Table 9, the flexural strength is decreased upon impact in the low-energy regime as well as impact in the high-energy regime. The decrease of the flexural strength upon impact in the low-energy regime supports the occurrence of minor interior damage in the low-energy regime.

The fact that the effect of impact on the surface resistance does not vary with the impact energy in a monotonic fashion complicates the use of the surface resistance as a damage indicator. In contrast, impact decreases the volume resistivity at all energies. This behavior of the volume resistivity is attractive. However, the volume resistivity only changes significantly upon impact when the energy is low (at or below 1770 J in Figure 13(a)). Furthermore, the measurement of the volume resistivity requires perimetric electrical contacts, which are less convenient for implementation to a concrete structure than contacts that are on one surface. For these reasons, the volume resistivity is not recommended for use as a damage indicator. Rather, the surface resistance is recommended.

The history of impacts affects the effect of impact on the surface resistance. The behavior mentioned above (Figure 5(a)), is for the case of the impact energy being progressively increased, so that any impact is at an energy that is higher than that of all prior impacts. It is only in this case that the decrease of the surface resistance upon impact is observed in the high-energy regime. In the case that the impact energy is progressively decreased from 3990 J (Figure 10(a)), so that any impact is at an energy that is lower than those of all prior impacts, the surface resistance increases upon every impact. That the resistance increases upon impact at the high energy of 3990 J in the latter case means that, when impact in the high-energy regime occurs without prior impact, the minor interior damage associated with increase in the extent of fiber–fiber contact essentially does not occur, while the superficial damage occurs. This is because the mechanism of increasing the extent of fiber–fiber contact requires multiple cycles of deformation, as shown upon fatigue loading (Fu and Chung, 1996), so that this type minor interior damage essentially does not occur when there is no prior impact. Therefore, in the near absence of prior impact, the surface resistance is a good indicator of damage, with a higher resistance corresponding to more damage.

In case of the impact energy being progressively decreased, the surface resistance essentially does not change upon impact after the initial few impacts (Figure 10(a)). This is because of the increasing occurrence of the minor interior damage that involves increase in the degree of fiber–fiber contact and that causes the surface resistance to decrease. Since this type of minor interior damage requires prior impacts for its occurrence, its occurrence increases as more impacts have occurred.

This interpretation is supported by the slight decrease of the surface resistance after a few impacts at progressively decreasing energy, as observed for type B PAN-based fiber specimens (Figure 10(c)).

At the same fiber content, Type B PAN-based carbon fiber gives much lower resistivity than type A PAN-based fiber. This is attributed to the difference in surface condition, which affects the ease of dispersion of the fiber in the cement. The difference in surface condition has not been identified, but it stems from the desizing heat treatment that has been experienced by Type A PAN-based fiber. Both fibers have been subjected to ozone treatment in this work. Ozone treatment has been reported to provide oxygen-containing functional groups on the fiber surface, thereby improving the hydrophilic character and promoting the fiber dispersion (Fu et al., 1998; Xu and Chung, 2000; Chung, 2005). At Type B PAN-based fiber may be able to provide competitive sensing ability if the fiber content is reduced from 0.5% by mass to cement, so that the resistivity is increased to the range 10^4–$10^5\,\Omega$ cm.

Since type A and type B PAN-based fibers are identical except that Type A is desized and Type B is unsized, this work has shown that sizing and desizing can affect greatly the performance of carbon fiber. Desizing may result in a residue on the surface of the fiber, so a desized fiber may differ in surface chemistry from an unsized fiber. Different methods and extents of desizing may have different effects. This work uses heating for desizing, but chemical methods may be used instead. Future work is needed to understand the effects of sizing and desizing in relation to the use of carbon fiber in cement-based materials.

It is simpler to use unsized fiber rather than desized fiber. However, among the three types of carbon fibers used in this study, only type A PAN-based fiber, which is sized, is still in the market. The other two types have been discontinued from production by the manufacturers.

This work has shown that carbon fiber reinforced mortar with resistivity 10^4–$10^5\,\Omega$cm is suitable for impact sensing. For concrete, which contains both fine and coarse aggregates, the suitable range of resistivity will probably shift upward a little (Wen and Chung, 2007c).

There are limitations to the practical use of carbon fiber cement-based materials as sensors. One limitation is the need for a reference measurement made prior to the damage infliction of concern. A higher value of the surface resistance would indicate a larger amount of cumulative damage, provided that the prior number of impacts is small (less than about 5), i.e., provided that damage is in the regime in which the surface resistance increases upon impact. Within this regime the resistance increase indicates the cumulative damage to the specimen, but does not give information on the history of impacts. A further limitation is that the point of impact must be between the voltage contacts. This implies that the distance between contacts should be large for the purpose of monitoring a large area of the structure. However, as noted in Section 'Effect of Length of Resistance Measurement Region,' the distance between contacts cannot be too large, due to the decrease in sensitivity with increasing contact separation. These two factors limit the range of distance between contacts in practical application.

Due to the above considerations, carbon fiber cement-based material is recommended for use as an impact damage sensor for structures that do not encounter impacts frequently. An example is a structure in the form of the column of a bridge. Impacts to the column are infrequent, but are important to be sensed. For such structures, the surface resistance is recommended as a damage indicator. The higher is the surface resistance, the more severe is the cumulative damage. In such structures, the carbon fiber cement-based material can be used to detect damage in its infancy. It may be used to detect damage too small to be detected by visual inspection (Figure 24) or ultrasonic methods. The detection of such small damage is of practical importance, because surface damage is prone to aggravation by abrasion, chemicals and weather.

The four-probe surface contact configuration (Figure 1(a)) provides the largest fractional change in resistance as compared to other contact configurations, but is more onerous to apply to structures as four contacts are needed. In contrast, the two-probe method requires only two contacts, though it gives lower sensitivity. The embedded steel wool contact would be the most difficult to install because it is placed within the cement mortar rather than being applied on the surface. The two-probe method involving silver paint contacts of large area, as shown in Figure 3(b), provides the second largest fractional change in resistance, but the large amount of silver paint needed can be costly. Alternatives to silver paint, such as colloidal graphite and nickel paint may be investigated. Such alternatives have a higher resistivity, but the cost is relatively low.

Moisture content is a known variable that affects the resistance of carbon fiber cement mortar. The fractional decrease in the resistivity of carbon fiber cement paste (without aggregate) due to saturated water ranges from 0.65 (Wen and Chung, 2008) to 0.93 (Wen and Chung, 2006d), relative to the value for the dry state. This degree of change due to moisture would overshadow the 0.23 (i.e., 23%) maximum fractional increase in longitudinal volume resistivity caused by impact damage (Table 6), though the effect of saturated water on the resistivity of mortar is expected to be less than that on the resistivity of cement paste. However, the 2.02 (i.e., 202%) maximum fractional increase in surface resistance due to impact damage (Table 6) is substantially larger than the above-mentioned fractional decrease due

to saturated moisture. Hence, the surface resistance change due to impact damage is expected to be a reliable indicator of damage, even in the presence of moisture.

CONCLUSIONS

Cement mortar containing short carbon fiber, silica fume (15% by mass of cement) and fine aggregate has been found to be effective for sensing its own impact damage through the effect of impact on the DC or AC electrical resistance, provided that the region of resistance measurement contains the point of impact. This region can be of length 25–203 mm in the direction of resistance measurement, but the maximum length has not been determined. The longer the region, the less is the damage sensitivity. The carbon fiber mortar may be in bulk form or in the form of a coating of thickness as small as 5 mm.

The carbon fiber can be made from pitch or PAN, provided that the resistivity of the mortar is in the range 10^4–$10^5\,\Omega$cm, as attained by pitch-based carbon fiber (15 μm diameter, 5 mm long, unsized) at 0.5% or 1.0% by mass of cement or by type A PAN-based carbon fiber (7 μm diameter, 8 mm long, desized) at 0.5% by mass of cement. Due to the low mortar resistivity of $10^3\,\Omega$cm, pitch-based carbon fiber at 1.5% by mass of cement and type B PAN-based carbon fiber (7 μm diameter, 8 mm long, unsized) at 0.5% by mass of cement are less effective. In the absence of fiber, there is no sensing ability.

The surface resistance measured at the surface receiving the impact is a particularly effective indicator of the impact damage, as shown for impact energy 880–3990 J. Due to impact at energy up to 2660 J, for example, the flexural strength decrease is 20%, the flexural toughness decrease is 81% and the indent depth is 64 μm, with no visible cracks, as shown for pitch-based carbon fiber at 0.5% by mass of cement. Compared to DC, AC (equivalent circuit with resistor and capacitor in series) tends to give lower surface resistance for the undamaged state and higher fractional increase in the surface resistance upon damage. The oblique resistance and the longitudinal volume resistance are much less effective, due to the dominance of damage in the surface region.

The four-probe method gives higher fractional increase in the surface resistance upon damage than the two-probe method, although the two-probe method gives adequate sensing when the area of each of the two electrical contacts is sufficiently large (e.g., 2700 mm^2). Electrical contacts can be made of silver paint or embedded steel wool.

The surface resistance increases abruptly upon impact, though it decreases abruptly upon impact after a sufficient number (5–40) of impacts have been inflicted. The higher is the impact energy, the smaller is the number of impacts needed to change from the abrupt increase behavior to the abrupt decrease behavior. The abrupt increase is due to the increase in resistivity upon damage. The resistivity of the damaged region is 1800% higher than that of the undamaged state for 2660 J and the pitch-based carbon fiber. On the other hand, the abrupt decrease is due to the subtle damage of the cement matrix between adjacent fibers and the consequent increase in the degree of fiber–fiber contact and decrease in the resistivity, as previously reported upon fatigue damage. When the impact energy is higher than that of prior impacts, the impact damage sensitivity is better than the case of the impact energy being lower than that of prior impacts.

ACKNOWLEDGMENT

This research was supported in part by Global Contour Ltd. under the Army SBIR grant (Program Manager: Dr Jaycee Chung).

REFERENCES

Bontea, D.-M., Chung, D.D.L. and Lee, G.C. 2000. "Damage in Carbon Fiber Reinforced Concrete, Monitored by Electrical Resistance Measurement," *Cement and Concrete Research*, 30(4):651–659.

Cao, J. and Chung, D.D.L. 2001. "Degradation of the Bond between Concrete and Steel under Cyclic Shear Loading, Monitored by Contact Electrical Resistance Measurement," *Cement and Concrete Research*, 31(4):669–671.

Cao, J. and Chung, D.D.L. 2004. "Electric Polarization and Depolarization in Cement-based Materials, Studied by Apparent Electrical Resistance Measurement," *Cement and Concrete Research*, 34(3):481–485.

Chen, P.-W. and Chung, D.D.L. 1993a. "Carbon Fiber Reinforced Concrete as a Smart Material Capable of Non-destructive Flaw Detection," *Smart Materials and Structures*, 2:22–30.

Chen, P.-W. and Chung, D.D.L. 1993b. "Carbon Fiber Reinforced Concrete as an Electrical Contact Material for Smart Structures," *Smart Materials and Structures*, 2(3):181–188.

Chen, P.-W. and Chung, D.D.L. 1995. "Improving the Electrical Conductivity of Composites Comprised of Short Conducting Fibers in a Non-conducting Matrix: the Addition of a Non-Conducting Particulate Filler," *Journal of Electronic Materials*, 24(1):47–51.

Chen, P.-W. and Chung, D.D.L. 1996. "Concrete as a New Strain/Stress Sensor," *Composites, Part B*, 27B:11–23.

Chen, B., Wu, K. and Yao, W. 2004. "Conductivity of Carbon Fiber Reinforced Cement-based Composites," *Cement and Concrete Composites*, 26:291–297.

Chung, D.D.L. 2002a. "Piezoresistive Cement-based Materials for Strain Sensing," *Journal of Intelligent Material Systems and Structures*, 13(9):599–609.

Chung, D.D.L. 2002b. "Electrical Conduction Behavior of Cement-Matrix Composites," *Journal of Materials Engineering and Performance*, 11(2):194–204.

Chung, D.D.L. 2003. "Damage in Cement-based Materials, Studied by Electrical Resistance Measurement," *Materials Science & Engineering Research*, 42(1):1–40.

Chung, D.D.L. 2004. "Electrically Conductive Cement-based Materials," *Advances in Cement Research*, 16(4):167–176.

Chung, D.D.L. 2005. "Dispersion of Short Fibers in Cement," *Journal of Materials in Civil Engineering*, 17(4):379–383.

Fu, X. and Chung, D.D.L. 1995. "Carbon Fiber Reinforced Mortar as an Electrical Contact Material for Cathodic Protection," *Cement Concrete Research*, 25(4):689–694.

Fu, X. and Chung, D.D.L. 1996. "Self-Monitoring of Fatigue Damage in Carbon Fiber Reinforced Cement," *Cement Concrete Research*, 26(1):15–20.

Fu, X. and Chung, D.D.L. 1997. "Effect of Curing Age on the Self-monitoring Behavior of Carbon Fiber Reinforced Mortar," *Cement Concrete Research*, 27(9):1313–1318.

Fu, X., Lu, W. and Chung, D.D.L. 1998. "Ozone Treatment of Carbon Fiber for Reinforcing Cement," *Carbon*, 36(9):1337–1345.

Leong, C. and Chung, D.D.L. 2006. "Improving the Electrical and Mechanical Behavior of Electrically Conductive Paint by Partial Replacement of Silver by Carbon Black," *Journal Electronic Materials*, 35(1):118–122.

Reza, F., Batson, G.B., Yamamuro, J.A. and Lee, J.S. 2003. "Resistance Changes During Compression of Carbon Fiber Cement Composites," *Journal of Materials in Civil Engineering*, 15(5):476–483.

Wang, S. and Chung, D.D.L. 2005. "The Interlaminar Interface of a Carbon Fiber Epoxy-Matrix Composite as an Impact Sensor," *Journal Material Science*, 40:1863–1867.

Wang, D. and Chung, D.D.L. 2006. "Comparative Evaluation of the Electrical Configurations for the Two-dimensional Electric Potential Method of Damage Monitoring in Carbon Fiber Polymer-Matrix Composite," *Smart Materials and Structures*, 15:1332–1344.

Wang, S., Chung, D.D.L. and Chung, J.H. 2005a. "Effects of Composite Lay-up Configuration and Thickness on the Damage Self-sensing Behavior of Carbon Fiber Polymer-Matrix Composite," *Journal Material Science*, 40(2):561–568.

Wang, S., Chung, D.D.L. and Chung, J.H. 2005b. "Impact Damage of Carbon Fiber Polymer-Matrix Composites, Monitored by Electrical Resistance Measurement," *Composites: Part A*, 36:1707–1715.

Wang, S., Chung, D.D.L. and Chung, J.H. 2005c. "Self-sensing of Damage in Carbon Fiber Polymer-Matrix Composite by Measurement of the Electrical Resistance or Potential Away from the Damaged Region," *Journal Material Science*, 40(24):6463–6472.

Wang, S., Chung, D.D.L. and Chung, J.H. 2006a. "Self-sensing of Damage in Carbon Fiber Polymer-Matrix Composite Cylinder by Electrical Resistance Measurement," *Journal of Intelligent Material Systems and Structures*, 17(1):57–62.

Wang, D., Wang, S., Chung, D.D.L. and Chung, J.H. 2006c. "Comparison of the Electrical Resistance and Potential Techniques for the Self-Sensing of Damage in Carbon Fiber Polymer-Matrix Composites," *Journal Intelligent Material Systems Structures*, 17(10):853–861.

Wang, D., Wang, S., Chung, D.D.L. and Chung, J.H. 2006d. "Sensitivity of the Two-dimensional Electric Potential/ Resistance Method for Damage Monitoring in Carbon Fiber Polymer-Matrix Composite," *Journal Material Science*, 41(15):4839–4846.

Wang, S., Pang, D.S. and Chung, D.D.L. 2007. "Hygrothermal Stability of Electrical Contacts Made from Silver and Graphite Electrically Conductive Pastes," *Journal Electronic Materials*, 36(1):65–74.

Wang, S., Wang, D., Chung, D.D.L. and Chung, J.H. 2006b. "Method of Sensing Impact Damage in Carbon Fiber Polymer-Matrix Composite by Electrical Resistance Measurement," *Journal Material Science*, 41(8):2281–2289.

Wang, S., Wen, S. and Chung, D.D.L. 2004. "Resistance Heating Using Electrically Conductive Cements," *Advanced Cement Research*, 16(4):161–166.

Wen, S. and Chung, D.D.L. 1999. "Carbon Fiber-reinforced Cement as a Thermistor," *Cement Concrete Research*, 29(6):961–965.

Wen, S. and Chung, D.D.L. 2000. "Uniaxial Tension in Carbon Fiber Reinforced Cement, Sensed by Electrical Resistivity Measurement in Longitudinal and Transverse Directions," *Cement Concrete Research*, 30(8):1289–1294.

Wen, S. and Chung, D.D.L. 2001a. "Uniaxial Compression in Carbon Fiber Reinforced Cement, Sensed by Electrical Resistivity Measurement in Longitudinal and Transverse Directions," *Cement and Concrete Research*, 31:2297–2301.

Wen, S. and Chung, D.D.L. 2001b. "Carbon Fiber-reinforced Cement as a Strain-Sensing Coating," *Cement and Concrete Research*, 31(4):665–667.

Wen, S. and Chung, D.D.L. 2001c. "Electric Polarization in Carbon Fiber Reinforced Cement," *Cement and Concrete Research*, 31(2):141–147.

Wen, S. and Chung, D.D.L. 2003. "A Comparative Study of Steel- and Carbon-fibre Cement as Piezoresistive Strain Sensors," *Advance in Cement Research*, 15(3):119–128.

Wen, S. and Chung, D.D.L. 2005. "Strain Sensing Characteristics of Carbon Fiber Reinforced Cement," *ACI Material Journal*, 102(4):244–248.

Wen, S. and Chung, D.D.L. 2006a. "Spatially Resolved Self-sensing of Strain and Damage in Carbon Fiber Cement," *Journal Material Science*, 41(15):4823–4831.

Wen, S. and Chung, D.D.L. 2006b. "Self-Sensing of Flexural Damage and Strain in Carbon Fiber Reinforced Cement and Effect of Embedded Steel Reinforcing Bars," *Carbon*, 44(8):1496–1502.

Wen, S. and Chung, D.D.L. 2006c. "Effects of Strain and Damage on the Strain Sensing Ability of Carbon Fiber Cement," *Journal Material Civil Engineering*, 18(3):355–360.

Wen, S. and Chung, D.D.L. 2006d. "The Role of Electronic and Ionic Conduction in the Electrical Conductivity of Carbon Fiber Reinforced Cement," *Carbon*, 44:2130–2138.

Wen, S. and Chung, D.D.L. 2007a. "Electrical-Resistance-based Damage Self-sensing in Carbon Fiber Reinforced Cement," *Carbon*, 45(4):710–716.

Wen, S. and Chung, D.D.L. 2007b. "Piezoresistivity-based Strain Sensing in Carbon Fiber Reinforced Cement," *ACI Material Journal*, 104(2):171–179.

Wen, S. and Chung, D.D.L. 2007c. "Double Percolation in the Electrical Conduction in Carbon Fiber Reinforced Cement-based Material," *Carbon*, 45(2):263–267.

Wen, S. and Chung, D.D.L. 2008. "Effect of Moisture on Piezoresistivity of Carbon Fiber-reinforced Cement Paste," *ACI Material Journal*, 105(3):274–280.

Xu, Y. and Chung, D.D.L. 2000. "Cement-Based Materials Improved by Surface Treated Admixtures," *ACI Material Journal*, 97(3):333–342.

Yao, W., Chen, B. and Wu, K. 2003. "Smart Behavior of Carbon Fiber Reinforced Cement-based Composite," *Journal Material Science Technology*, 19(3):239–243.